NASA TECHNICAL NOTE

NASA TN D-2597

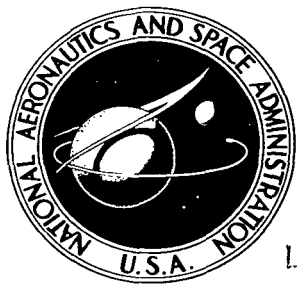

NASA TN D-2597

AN EXPERIMENTAL EVALUATION OF ARRAY OF THREE ELECTRON-BOMBARDMENT ION THRUSTORS

by Eugene V. Pawlik

Lewis Research Center
Cleveland, Ohio

NATIONAL AERONAUTICS AND SPACE ADMINISTRATION • WASHINGTON, D. C. • JANUARY 1965

AN EXPERIMENTAL EVALUATION OF ARRAY OF THREE ELECTRON-BOMBARDMENT ION THRUSTORS

By Eugene V. Pawlik

Lewis Research Center
Cleveland, Ohio

NATIONAL AERONAUTICS AND SPACE ADMINISTRATION

For sale by the Office of Technical Services, Department of Commerce,
Washington, D.C. 20230 -- Price $2.00

AN EXPERIMENTAL EVALUATION OF ARRAY OF THREE ELECTRON-BOMBARDMENT ION THRUSTORS

by Eugene V. Pawlik

Lewis Research Center

SUMMARY

Three 20-centimeter-diameter electron-bombardment ion thrustors mounted in a close lateral array were used in a systematic investigation of steady-state interaction between thrustors, ion-beam neutralization, and beam spreading. The thrustors used mercury as the propellant and were operated at 4500 volts net accelerating potential and at beam currents that ranged from 0.75 to 3.0 amperes for the array. No significant electrical interaction between thrustor modules was observed.

Neutralization of the ion beam was accomplished with three immersed emitter-type neutralizers consisting of twisted tantalum wires strung across the diameter of each module. A beam collector was electrically isolated from the vacuum tank so that the effectiveness of the neutralizers could be determined. Beam potentials were approximately determined by measuring the collector potential. A neutral exhaust beam could be achieved with any neutralizer that was coupled to the aggregate beam through the plasma.

A rake of impingement probes that could be swept through the exhaust of the array was used to determine beam spreading. Mean cone angles of about 10° existed for each thrustor. Skew of the thrust vector was noticeable for most modules. Thrust levels as high as 0.393 newton (88 millipounds) were achieved by the array.

INTRODUCTION

Research on the electron-bombardment ion thrustor has progressed to a point where it is appropriate to investigate the feasibility, performance, and operating characteristics of multithrustor systems. For a given design value of specific impulse, particularly in the lower range of interest, the close spacing of accelerator electrodes in ion thrustors tends to limit thrustor size. Even with the 50-centimeter-diameter thrustor reported in references 1 and 2, multimodule arrays would be necessary to provide jet powers of the magnitude required for primary propulsion.

Preliminary investigations have established the feasibility of operating arrays of

from three to nine electron-bombardment thrustors, and this work is reported in references 1, 3, and 4. The present investigation is a more detailed study of the operating characteristics and performance of a linear array of three 20-centimeter-diameter electron-bombardment thrustors.

Interactions between thrustors in the array were determined by observing the operation of the center thrustor as major changes were made in the operating conditions of the two outer thrustors. Neutralization and neutralizer interaction were investigated to evaluate these phenomena under various operating modes. Beam profiles were also studied to determine the effects of beam spreading and exhaust-beam skew on the performance of an array.

Electrical parameters within the thrustors were measured and monitored with standard instrumentation. Space environment was simulated to a degree through the use of an exhaust-beam collector that was electrically isolated from the vacuum tank and thrustor array. This collector was of particular importance in the beam-neutralization measurements. Current-density profiles in the exhaust beams from the array were measured with a movable rake of impingement probes.

APPARATUS

Thrustors

The three electron-bombardment ion thrustors used in this study produced 20-centimeter-diameter exhaust beams. One of the thrustors is shown in the cutaway drawing in figure 1. (The downstream neutralizer location is not indicated.) During thrustor operation, mercury was vaporized in an electrically heated vaporizer of the type described in reference 5. Propellant vapor was supplied at a steady rate through a porous stainless-steel restriction within the vaporizer by holding the temperature constant. A flow distributor provided a relatively uniform influx of vapor to the ion chamber. The distributor consisted of a plate having twenty 1.3-centimeter-diameter holes that were evenly spaced on 8.0- and 12.0-centimeter-diameter circles, 10 holes per circle. The ion chamber contained the cylindrical anode (20 cm in diam. and 15 cm long). The electron emitter or cathode, was a V-shaped tantalum filament located on the axis of the chamber. During operation, electrons from the filament were accelerated toward the anode, producing ionizing collisions with the mercury vapor and filling the chamber with a plasma. The ion-chamber potential difference (discharge voltage) was normally 50 volts. An approximately axial magnetic field was used to contain the ionizing electrons and was produced by a coil wound about the outside of the thrustor.

The ion-accelerating structure (screen and accelerator grids) at the downstream end

of the chamber extracted ions from the plasma and accelerated them to produce an exhaust beam. Nonionized atoms could diffuse through the accelerator plate openings into the vacuum tank. Aluminum oxide balls supported and positioned the accelerator grids, which consisted of a match drilled set of 0.155-centimeter-thick molybdenum plates with 0.475-centimeter-diameter holes on 0.635-centimeter equilateral hole spacing.

The thrustors in this study were similar to the 20-centimeter-diameter thrustor described in reference 6 and identical to the largest unit presented in reference 7. Differences between the units of these two references exist in the geometry of the distributor and the shape of the magnetic field. Additional description of individual thrustor operation is presented in reference 8.

The thrustor array consisted of three thrustors mounted side by side in a straight line with centerline spacings of 32.1 centimeters. The thrustor installation is shown in figure 2. The modules are numbered 1, 2, and 3, as depicted in the figure.

The three thrustors were operated from two high-voltage power supplies that provided the net accelerating voltage V_I and accelerator voltage V_A for the array. High-voltage circuit breakers were used to supply accelerating voltage or isolate a faulted thrustor. Separate low-voltage supplies were used for each thrustor to supply cathode and vaporizer heating, magnetic field, and discharge voltage. A schematic drawing of the power supplied, thrustor electrical connections, and metered variables is shown in figure 3. Studies of this circuit and similar circuits under conditions of electrical breakdown are presented in references 3 and 4.

Neutralization of the ion beams was accomplished by three immersed emitter-type neutralizers. Each consisted of two 0.8-millimeter-diameter tantalum wires twisted together and strung across the center of each exhaust beam 5.0 centimeters downstream of the accelerator plates. The neutralizers were all biased at the same potential above ground by a common voltage supply to prevent electrons from streaming from the neutralizer to the tank walls.

Vacuum System and Ion-Beam Instrumentation

A cutaway view of the vacuum facility and the thrustor mounting is shown in figure 4. The three ion thrustors were mounted within a thrustor compartment 10 feet in diameter and 10 feet long that could be isolated from the 25-foot-diameter by 70-foot-long main vacuum tank by a 10-foot-diameter gate valve. Protective screening (see fig. 2) was mounted around the array to prevent the dilute plasma, which fills the tank during thrustor operation, from introducing spurious current readings into the electrical system. Although it was possible to bias the plasma shielding, negative if desired, for the data in this report, the screen was grounded. A grounded screen has been adequate to stop elec-

tron backstreaming.

The vacuum system is evacuated by twenty-two 32-inch oil-diffusion pumps, two of which are located on the thrustor compartment. Each pump contains a liquid-nitrogen-cooled baffle to prevent oil backstreaming. A liquid-nitrogen-cooled honeycomb surface containing an area of 2600 square meters is mounted in the facility to condense the thrustor exhaust beam. The interior of the vacuum facility showing the cryobaffle is presented in figure 5. The photograph was taken prior to the installation of the ion-beam collector.

Pressures within the main vacuum tank were about 2×10^{-7} torr when the thrustors were not operating. During testing, the pressures, which were approximately equal in the tank and thrustor compartment, rose about one decade.

Seventeen impingement probes of the type described in reference 9 were used to obtain ion-beam density profiles. The maximum error due to secondary electron emission was probably less than 10 percent for 4000-electron-volt heavy ions on a molybdenum surface (ref. 10). The probes were mounted 15.25 centimeters apart on a 3.7-meter-long arm that was pivoted about one end (see fig. 6). A servomotor was used to sweep the rake through an angle of 75°. The 1.20-centimeter-diameter molybdenum probes (biased at -24 volts to repel electrons) were located in a plane 1.0 meter downstream of the accelerator surfaces. The ion-beam current density was recorded on strip charts along with a position indication of the probe arm as the beam was traversed.

A segmented collector consisting of five stainless-steel annular sections was used for neutralization studies (see fig. 4). It had an outer diameter of 4.57 meters. The axial location, which could be varied from 3.0 to 10.6 meters from the thrustor accelerator surfaces, was determined optically from a scale marked on the tank wall near the collector. Ion currents to each annular section of the collector could be measured, or it could be electrically isolated for beam-neutralization measurements as described in reference 11. The collector could be biased to repel electrons when used to measure segment currents. A schematic drawing of the collector and impingement probe systems is shown in figure 7.

When the thrustors were operating, data were obtained from panel-meter readings, strip-chart recordings, and by notation or photographing oscilloscope waveforms. Isolation of the panel meters from the high voltages was accomplished through instrument amplifiers. Some d-c drift existed within the metering system, and therefore meters were calibrated before and after each run. Meter accuracy was about 5 percent for all readings presented. The accuracy of the ion-thrustor-current meter readings was continuously checked during a run by summation meter readings of total thrustor and ion-beam currents $\left(\sum J_+ = J_{+1} + J_{+2} + J_{+3}, \sum J_B = \sum J_+ - \sum J_A, \text{ see fig. 3}\right)$. (All symbols are defined in appendix A.)

PROCEDURE

The thrustors were placed in operation by applying all operating voltages and then by heating the propellant vaporizers. Individual thrustors were operated at beam currents ranging from 0.25 to 1.00 ampere. Most of the data presented were obtained at an anode or net accelerating voltage (measured with respect to ground) of 4500 volts and an accelerator voltage of -1500 volts. Prior to and after each test, the grid spacing was measured at nine locations. Average surface-to-surface grid spacings of about 0.25 centimeters were used in the tests reported herein.

During each data run, the vaporizer temperatures were adjusted so that the propellant utilization was 80 percent or slightly higher for each unit. The neutral mercury flow rate was determined from values of ion-beam current ($J_+ - J_A$) and filament-emission current together with the performance map of figure 8. Figure 8 is reproduced from reference 7 and was obtained with calibrated orifices and a steam-heated vaporizer during single-thrustor operation in a smaller vacuum facility. The performance-map data were obtained with anode and accelerator voltages and also a magnetic-field strength at different values from those used for the thrustor in this study. These differences lowered the level of the ion-beam current of the performance map slightly (about 6 percent as determined by the steady-state gain curves of ref. 7). This 6-percent correction was applied in computing propellant utilization. The vaporizer temperature was monitored during each run with an iron-constantan thermocouple mounted on the upstream side of the vaporizer. The temperature was adjusted so that the thrustor operation was within the 80- to 90-percent propellant-utilization region of the performance map at normal operating conditions (ΔV_I = 50 v, B = 14.5 gauss). The vaporizer temperature was then maintained near this predetermined value for the duration of the run. The open-loop control used for vaporizer heating was unable to provide close temperature regulation; hence, small operating deviations are reflected in the data.

Thrustor Interaction

Most of the interaction data for the array were obtained by a difference technique in order to minimize effects due to drifting in both the boiler temperature and in the d-c levels of the meter readings. Interaction was investigated by observing the operation of the center thrustor (thrustor 2) before and after major changes were made in the other two units. Discharge-voltage and magnetic-field effects were investigated in this manner. Accelerator performance was checked on the center unit with the array functioning in the manner just described and also with a single module operating for two values of

ion-beam current (0.25 and 0.50 amp).

Beam Neutralization

As described in reference 12, neutralizers are not necessary for thrustor operation within vacuum facilities because the ion thrustor is usually electrically connected to the tank through the beam. In this case the electrons from both the tank walls and the residual gas provide charge neutralization; therefore, current neutralization is not required except perhaps for more stable operation at low pressures (below 10^{-6} torr) (ref. 12). For the neutralization tests described herein, the array was operated with a severed ground return path for the ions arriving at the collector. The ion-beam collector, when separated from ground by a high-impedance path, serves as a surface on which ion-electron recombination occurs. The collector also serves as a convenient probe for approximate measurements of the plasma potential. These plasma measurements are useful in determining the coupling of the neutralizer to the beam. With the collector floating, the neutralizers are forced to operate and provide current neutralization.

The physical location of the collector during these tests was adjusted by metering the collector current as it was moved toward the array until the ion current it collected reached a value approximately equal to the total beam current. A distance of 4.57 meters from the accelerator plates was adequate to intercept nearly all of the beam for all conditions investigated, and the collector was therefore kept at this location during all neutralizer testing.

Neutralizer coupling to the ion beam was measured by determining the potential difference between the collector and neutralizer. This was accomplished by supplying the a-c heating current to the neutralizer filament through a diode so that only half of each 60-cycle waveform was used for heating. During the other half cycle, the neutralizer remained hot and emissive but did not experience a longitudinal voltage gradient, thus furnishing a unipotential point from which to make coupling measurements. All three neutralizers were in phase during the heating cycle.

During the neutralization tests the existence or lack of local charge concentration in the beam was investigated by comparative measurements of the exhaust-beam profiles under a variety of operating conditions. For example, impingement-probe traces for floating-collector operation were examined against profiles obtained a short time later with the thrustor at the same operating condition and with the collector grounded. Identical profiles were assumed to indicate similar charge distribution for each operating mode.

Neutralization tests were conducted with various combinations of thrustors and neutralizers operating. The voltage difference between neutralizer bias and collector poten-

tial was noted for each combination or thrustor power level. The metered variables were observed on oscilloscope traces and notations were made of the average values.

Beam Spreading and Alinement

Ion-beam spreading and direction were investigated by measuring ion current-density profiles in the exhaust beams. Ion-beam current-density profiles were obtained with the rake of impingement probes for both individual-unit and thrustor-array operation. Operating conditions of each thrustor were recorded from panel-meter readings during the probe-arm survey. The ion-impingement currents from each probe during a survey were recorded on strip charts as the beam was traversed.

RESULTS AND DISCUSSION

In the discussion that follows, the interaction investigations between operating modules at several power levels will be described. The effects due to each operating parameter are detailed. Ion-beam neutralization results for the array will then be considered followed by an examination of the exhaust-beam profiles.

Thrustor Interactions

Evidence of thrustor interaction was sought because beam spreading from single modules usually exists to some extent, and the resultant conducting plasma could electrically connect the thrustor modules. Thrustor coupling (through the ion beam) to the vacuum tank walls has been noted for single-unit operation during low-neutral-density conditions, at or below pressure readings of 10^{-6} torr. This operation has been typically accompanied by random sparks, particularly in the regions of the beam nearest to a conducting surface. As described in reference 13, these sparks introduced undesirable transients to the thrustor.

Interaction effects on accelerator performance were also investigated. Accelerator currents for the electron-bombardment thrustor consist, to some extent, of charge-exchange ions, as described in reference 14. Data were therefore obtained for the center thrustor alone and also under conditions of possible additional neutral propellant from nearby operating thrustors.

Discharge voltage. - During interaction tests the steady-state operation of the center unit was monitored as either the discharge voltage or the magnetic field of adjacent

thrustors was varied. Parameters were investigated over a 4 to 1 range of propellant flow rates from the vaporizer. Impingement-probe traverses of the beam taken during interaction testing indicated that, at a distance of 1 meter from the accelerator plates, beam spreading had always occurred to the extent that adjacent thrustors were in communication. Data for the center thrustor during thrustor interaction tests are presented in table I for module beam currents near 0.25, 0.50, 0.75, and 1.00 ampere. The anode or net accelerating voltage was maintained at 4500 volts for all of the data in table I and for most of the data presented in the report. This value corresponds to a specific impulse ($I = \eta_u \bar{v}/g$) of about 5500 seconds. The data in table I are presented in sets, each consisting of three lines. In each set the first line represents the center module, while the other two thrustors were operating at normal conditions and at nearly the same ion beam current. On the second line of the set the discharge voltage (runs 1 to 4) or the magnetic field (runs 5 to 8) were shut off for thrustor 1. On the third line the same parameter was nulled for both thrustors 1 and 3. The center thrustor data were obtained with discharge voltages of 25 to 90 volts as the other two units were either functioning at normal operating conditions or had the plasma extinguished ($\Delta V_I = 0$).

An indication of thrustor operation interaction can best be obtained by a calculation of the energy cost of producing a beam ion, because extraneous effects such as small fluctuations in thrustor operation and power-supply loading are then minimized. The calculation was made according to the equation $\mathscr{E} = \Delta V_I(J_I - J_B)/J_B$. Values of energy dissipated in the discharge chamber in electron volts per beam ion are presented in table I. This energy loss for ion beams of 0.50 and 0.75 ampere from the center thrustor is plotted against discharge voltage in figures 9(a) and (b), respectively. Interaction effects were negligible, as evidenced by the small spread of the data points between single and multithrustor operation. The faired curves in the figure, therefore, represent equally well either single-thrustor or array operation.

Magnetic field. - The thrustor interaction due to magnetic-field variations is included in the data of table I and is represented by runs 5 to 8. Turning off the magnetic field on a particular unit would result in a reduced beam output for that unit (about 20 percent of the value presented for J_B on the first line of the data set). Data were obtained for the center thrustor as its magnetic field was varied over a range from about 6.5 to 22.4 gauss as a nearly constant beam current was maintained. These data were taken with the magnetic field of the outer thrustors set at either 14.5 or 0 gauss. The polarity of the magnetic field was the same for all three units, and, therefore, the fields of the end units reduce the field at the center module slightly. By gaussmeter measurements, the center thrustor electromagnet currents presented in the table created a 1.3-gauss axial magnetic field at the middle of the center thrustor screen for each ampere of solenoid current. Figure 10 shows the discharge-chamber energy dissipation per

beam ion as a function of the electromagnetic current for the center module for beam currents of 0.50 and 0.75 ampere. Some data spread was present and was thought to be due primarily to the lack of close regulation of the vaporizer temperature. Interaction effects were negligible for the majority of the field strengths investigated.

A consistent trend was noticeable at low levels of magnetic-field strength (about 6.5 gauss) where the fields of the neighboring thrustors became significant with respect to the field of the center unit (about 4 percent of the field at the middle of the center electromagnet, as determined by gaussmeter measurements). A slight interaction was always noticeable at the low field strength, as evidenced by a decreased discharge-chamber energy and subsequent beam-current increase as the adjacent thrustor magnetic fields were reduced (see table I, runs 5 and 6). This low field operation could not be conveniently achieved at beam currents of 0.75 ampere or above, since the emission current required at these conditions exceeded the capabilities of the cathode used. A steep region exists in the functional relation between discharge energy and magnetic field at low-field intensity (fig. 10(a)). A small field change could, therefore, result in a noticeable difference in thrustor operation. Interaction of this type for the field strengths involved was not normally noticeable on the less sensitive (high field strength) region of the curves. With a close two-dimensional packing of the thrustors in a large array, however, the effect might be more pronounced.

Because thrustor operation itself is not sensitive to magnetic-field polarity, this magnetic-field interaction could be used to obtain a slight performance gain by placement of alternate polarity thrustors. The resulting increased magnetic field (7 to 13 percent) would improve the performance by reducing the discharge-chamber energy loss (20 to 40 ev/ion). Appendix B contains a brief analysis of the magnetic-field-strength increase that might be realized under large array conditions. Final flight configurations of thrustor arrays, however, may utilize permanent magnetic thrustors of the type described in reference 15. In this type of unit, the magnetic field exterior to the ionization chamber is restricted to high permeability paths and would therefore not affect the neighboring thrustors.

Although all possible thrustor interaction combinations are not presented in the data of table I, a wide range of conditions was investigated during the approximately 100 hours of array operation with no significant deviations from the results discussed. The results apply to steady-state conditions only, since transient effects were not investigated.

Accelerator interaction. - Accelerator impingement currents for the electron-bombardment thrustor are usually of the order of 1 percent of the beam current. The impingement current consists primarily of charge-exchange ions (ref. 14). The proximity of additional thrustors could produce an increased neutral density downstream of each module if a cosine distribution of the uncharged propellant exists at the accelerator

surface. The neutral propellant distribution for this assumed case and a typical beam spreading pattern are shown in sketch (a). If an additional supply of the low-velocity ion species were created within this downstream region and were attracted toward the accelerator surfaces, an interaction would be noticeable if the center thrustor accelerator current were monitored as alternate thrustors were turned off. Accelerator characteristic curves were obtained in a manner similar to that of reference 9. Accelerator currents were obtained at constant values of R (where R is defined as $V_I/(V_I + |V_A|)$, the ratio of net to total accelerating voltage) at beam-current levels of 0.25 and 0.50 ampere and are presented in table II (runs 9 and 10). Runs 9a and 10a are for array operation for which the total beam currents $\sum J_B$ were 0.75 (run 9a) and 1.50 amperes (run 10a), while runs 9b and 10b are for the center thrustor operating alone. In this mode the vaporizers on thrustors 1 and 3 were cold (no propellant flow). The accelerator currents obtained for both modes are plotted against the net accelerating potential for two values of beam current in figure 11. As the values of V_I and $|V_A|$ were lowered, keeping R constant, there was a sudden and steep rise in the accelerator impingement current. This sudden rise indicated that the plasma sheath shifted sufficiently to cause severe defocusing of the ion beams through the grid holes. From a comparison of the two modes of operation, no additional accelerator current, which could be attributed to an increase in charge-exchange ions, could be detected, since no consistent trend toward an increased accelerator current was present during three thrustor operations. Accelerator currents of 0.4 to 0.7 percent of the beam current were obtained on the center unit with or without the other two thrustors operating while it was functioning in the region of the curve where the plasma was correctly focused.

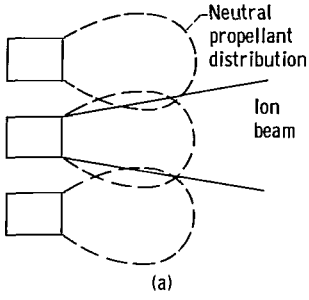

(a)

Beam-Neutralization Effects

Neutralization interactions and effectiveness were investigated by monitoring the collector potential and the neutralizer emission current during thrustor operation. For each operating point, the following three observations were taken as evidence of a neutralized exhaust beam:

(1) The absolute value of the emitted electron current equaled the ion-beam current, indicating current neutralization ($\sum J_B = \sum J_{NE}$).

(2) The potential of the floating collector (and thus the potential within the beam) was close to the neutralizer potential, indicating charge neutralization.

(No additional exhaust-beam spreading due to charge concentrations was evident.)

Before examining the data, a brief description of the potentials of interest and their

distribution will be useful for orientation purposes. The potential of the plasma along the length of the vacuum tank can be represented as shown in sketch (b). All voltages are measured with respect to ground.

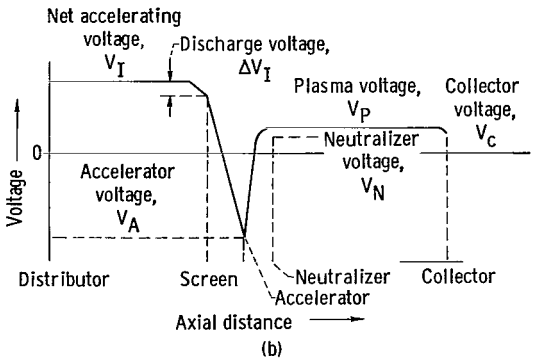

As described previously, with the collector floating, the neutralizers are forced to emit electrons in a manner similar to operation within a space environment. As long as charge neutralization is being accomplished, the tank plasma will be maintained at some voltage level V_P close to that of the neutralizer bias voltage V_N. A reasonable assessment of neutralization effectiveness therefore might be simply that the potential difference between the neutralizer and plasma be low (of the order of 15 v). The coupling between the plasma and the neutralizer can be expressed by the voltage difference necessary to extract the required number of electrons for current neutralization. This potential difference $V_P - V_N$ can be measured accurately by the emissive-probe techniques described in reference 11. As shown in reference 11, the coupling is approximately given by the potential difference between the ion-beam collector and the neutralizer $V_C - V_N$. This coupling indication is approximate due to the presence of a plasma sheath at the collector surface that could affect the measurement reading by several volts. Since it was not considered within the scope of this project to make refined measurements of the state of neutralization or degree of coupling by the plasma potential but simply to ascertain whether neutralization was indeed being accomplished, the less precise method was used. The results listed in table III therefore represent approximate values of plasma coupling. Levels of the collector voltage of 3 to 14 volts, positive relative to the neutralizer bias, were obtained. It has been shown in reference 11 that a sheath can vary from about 0 to 7 volts above the collector potential depending on the coupling of the neutralizer to the beam. If a constant sheath voltage as high as 7 volts existed for the data presented in this study, the plasma voltage could have ranged from 10 to 21 volts relative to the neutralizer.

The collector potential was obtained by recording oscilloscope traces as half wave rectified heating current was applied to the neutralizer. Typical waveforms obtained with the collector floating are presented in figure 12. Figure 12(a) is the neutralizer voltage waveform, while figures 12(b) to (d) represent the resulting collector voltages. There is no correspondence between time scales in figures 12(a) to (d). The collector traces correspond in order to the first three data points of run 13 (table III). The collector potential for most of the data was defined by a level region, as can be seen in figure 12(b). The effects of the potential gradient along the neutralizer during the heating

cycle are evidenced by the distorted half cycle sine wave. As the average value of the heating voltage of the neutralizer was reduced, cooling occurred to the extent that the neutralizer emission current might become temperature limited. As this happened, a rounding off at the end of the level region of the collector potential was evident. This rounding off occurred just prior to the heating cycle (fig. 12(c)). During some conditions, a fluctuation of the plasma voltage with time was observed in the collector waveform (fig. 12(d)). Because this condition was observed only when the emission current of neutralizers 2 and 3 exceeded 0.50 ampere and the frequency of these small perturbances was 60 cycles per second, it was assumed to be a neutralizer supply phenomenon and not an indication of an instability in the plasma.

The data presented in table III represent single-thrustor operation with individual neutralizers functioning (run 11) and combinations of thrustor and neutralizer operation (runs 12 to 14). Most of the multiple-unit data was obtained at approximately 0.25 ampere beam current per thrustor with some 0.50-ampere beam data presented in run 14. Two-thrustor data are presented in run 12 and three-thrustor data in run 13. Beam neutralization was achieved as long as a heated neutralizer was connected to the aggregate exhaust beam by the plasma of an operating module. Impingement probe traces, taken under neutralized conditions, indicated that each individual exhaust beam spread to the extent that beam overlapping of any two thrustors always occurred within a distance of 2 meters downstream of the accelerator plane.

In each combination presented in table III, neutralization was determined by the three conditions set forth at the beginning of this section. The third condition was established by probe traces obtained during floating-collector operation. These traces were, within the accuracy of the measuring device, identical to the traces obtained a short time later (2 to 3 min) with the collector grounded. Those obtained with the collector tied to ground represent a different mode of neutralization where secondary electrons were available over the collector surface. Because the probability of identical charge distribution with the resulting corresponding impingement probe traces seemed small, agreement of the traces under the two neutralization modes seemed to represent a lack of charge concentration in either case. Disturbing influences of the probe arm during the sweep were not noticeable in the collector waveform and were felt to be negligible. Beam spreading with the neutralizers unheated and the collector floating was easily detected by the method just described. Surprisingly, however, the thrustor operation was maintained in this condition. This was felt to be due to an ion charge concentration that was built up in front of the collector and contact by the beam with the vacuum tank walls was established as shown in sketch (c). For this case, however, thrustor operation was erratic with

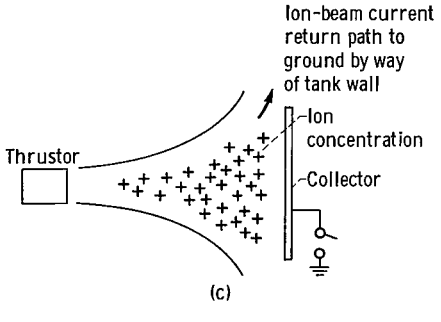

(c)

constant breakdown present and a high, noisy voltage level present on the collector.

In run 11 each of the neutralizers was operated in the space-charge-limited mode. Collector-neutralizer potential differences of about 3 volts were obtained for each unit at a beam current of approximately 0.25 ampere. These voltage measurements are plotted as a function of beam current in figure 13. Since the neutralizer was operating space-charge-limited surrounded by a constant plasma voltage V_P at a plasma sheath radius r, the approximate neutralizer current in amperes can be obtained from an expression for the space-charge-limited current of a diode with long concentric cylindrical electrodes (ref. 16):

$$J_{NES} = 14.7\times10^{-6}\,\frac{\ell(V_P - V_N)^{3/2}}{r\beta^2}$$

$$= C(V_P - V_N)^{3/2}$$

$$\simeq C(V_c - V_N)^{3/2} \qquad (1)$$

If the perveance C of the system remained constant, the plasma potential would vary with the emission current. A curve of constant perveance has therefore been faired through the data of figure 13. Constant perveance operation of the neutralizer is indicated within the accuracy of the data. Plasma sheath distances around the neutralizer would therefore be invariant, and the coupling of the beam to the neutralizer would be a function of the beam current.

During multiple-thrustor operation, the neutralizers of operating thrustors were always capable of supplying the required electrons to achieve neutralization. When two or more neutralizers were used, however, an interaction between them was evident. This interaction was primarily a result of the current neutralization requirement $\sum J_B = \sum J_{NE}$. Each neutralizer, therefore, contributed electrons in relation to the temperature at which it was operated and the extraction potential that was exerted by the plasma.

Data for two-thrustor operation during neutralization testing are presented in run 12 (table III) for several combinations of conditions. Best coupling to the plasma was always obtained when each thrustor was supplied electrons from its neutralizer. The coupling of each neutralizer to the beam was a function of the immersed-wire temperature, so that the emission-current load on each neutralizer could be varied with the heating current cycle imposed on it. With two neutralizers operating, it was possible to have one operating emission-limited, while the other was operating space-charge-limited. The

emission-limited current would operate according to the Richardson equation (ref. 17):

$$J_{NE} = AT^2 e^{\alpha/K_e - \varphi/KT}$$

When the neutralizers were operated in the space-charge-limited region, as described by equation (1), an unbalance of emission current was noted. The neutralizer heated to the highest temperature would always supply the greatest amount of current. Balanced operation ($J_{B,1} = J_{NE,1}$, $J_{B,2} = J_{NE,2}$, $J_{B,3} = J_{NE,3}$) could be achieved when approximately the same heating current was supplied to each strand of wire. This condition is believed to be due to an effective voltage that exists across the plasma sheath of each neutralizer. This effective voltage is a function of neutralizer temperature that also affects the thermal velocity of the emitted electrons. A similar effect is analyzed in reference 18 for the case of a cylindrical diode.

Complete array operation at low levels of beam current is presented in run 13 (table III). Various combinations of neutralizers and neutralizer-emission-current levels were used. Collector-neutralizer potential differences for this run are plotted in figure 14 as a function of the number of neutralizers being heated. Coupling is improved with the number of neutralizers used. As the emission-current load is balanced, a minimum collector-neutralizer is obtained with a fixed number of neutralizers operating.

Some of the results obtained at low beam-current levels in runs 12 and 13 were repeated for a higher beam current, and these results are presented in run 14. The results obtained were similar to those at the lower beam-current level except for a slight increase in the collector-neutralizer voltage level, which might be expected if a constant neutralizer perveance existed.

Plasma voltages indicated in these tests represent satisfactory levels of coupling between the neutralizer and the plasma. The lower values are more desirable, since they represent close electrical coupling, and their effect on thrust and power efficiency of the array is reduced, as is evident from the following one-dimensional relations

$$F = \dot{m}\bar{v} = \sqrt{2\frac{m}{q}(V_I - V_P)}\sum J_B$$

and

$$\eta_P = \frac{P_B}{P_T}$$

where

$$P_B = (V_I - V_P) \sum J_B$$

Since V_P is of the order of 10^{-3} V_I, small reduction in the preceding expressions is obtained under all of the beam-neutralization conditions examined.

High values of the plasma potential represent high electron injection energies that possibly could be reflected in beam noise and subsequent communication interference. High values of plasma potential could also be detrimental to neutralizer lifetime due to charge-exchange erosion (ref. 19).

In summary, neutralization was easily achieved during the operation of the thrustor array. By comparative measurements, best control of the exhaust plasma was obtained when the neutralizer of each operating thrustor was functioning. Penalties for single-neutralizer operation seemed small from the standpoint of thrust and efficiency losses; however, neutralizer power efficiency and lifetime were not considered, because the neutralizers used were not optimum designs. Interaction among neutralizers was present in that the neutralizer at the highest temperature supplied the most electrons emitted. The plasma potential was affected by the number of neutralizers in operation.

Beam Spreading and Alinement

Impingement probe traces of the exhaust beam were obtained with the array operating at beam-current levels of 0.25 to 1.00 ampere per thrustor. Ion-density profiles were recorded on strip charts as the rake of impingement probes was swept through the beam during individual-unit and thrustor-array operation. Panel-meter readings of the thrustor performance were also obtained during the probe sweep, and these data are presented in table IV. A total of four surveys was taken for each run corresponding to single-thrustor operation of units 1, 2, and 3 and simultaneous operation of 1, 2, and 3. The operation of each ion chamber was unchanged during a run as ions were extracted from only one module or the entire array. Ions could be accelerated from any desired module by the high-voltage switches shown in figure 3. Propellant utilization was determined for each impingement-probe sweep from the performance map of figure 9. Since $V_P \ll V_I$, thrust of the array was calculated from the equation

$$F = \sum J_B \sqrt{\frac{2m}{q} V_I}$$

Thrust levels as high as 0.393 newton were obtained.

Two probe traces were used to construct beam-density contour maps of the exhaust beam. These maps are presented in figure 15 for the four levels of beam power for each

thrustor. Each profile obtained approached the zero-intensity base line asymptotically, so therefore the intensity levels at zero and one on each contour map are appropriate. Some beam spread, skewness, and distortion were present in each case and are most clearly evident for single-thrustor operation. Since these conditions contribute toward the loss of thrust and represent a perturbing force on the net thrust vector of the array, the magnitude of these effects was examined.

Beam spreading was felt to be due to accelerator optics and was somewhat variant with beam-current level. Probe traces for the probe passing closest to the center of the contour map are presented in figure 16 for the center thrustor operating alone. Beam currents ranged from 0.25 to 1.00 ampere. A mean divergence angle was determined for these profiles to define approximately the beam spreading, since a well-defined beam edge did not exist. This angle θ was computed in a manner similar to that used in reference 10 and is defined by the equation

$$\langle \tan \theta \rangle = \frac{\int j_B \tan \theta \, d\omega}{\int j_B \, d\omega}$$

The integration was performed by dividing the profiles into small annular segments, where the current to each segment is j_B. The focal point from which the beam was apparently spreading was determined on the basis of an assumed uniform beam-density distribution at the accelerator plates. This focal-point distance is described by

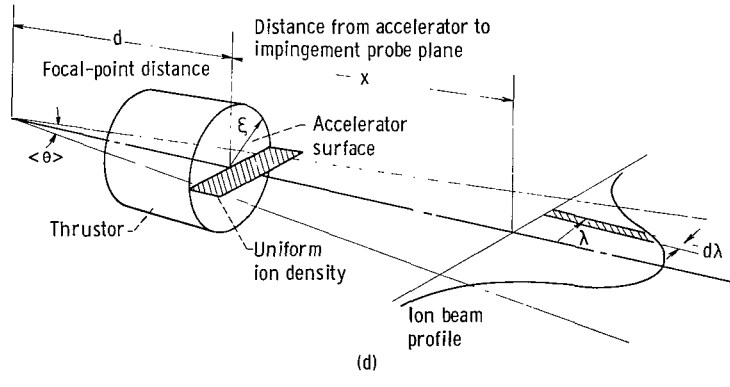

(d)

sketch (d). The mean divergence angle for the profile can therefore be represented as

$$\langle \tan \theta \rangle = \frac{1}{x + d} \frac{\int \lambda j_B \, d\omega}{\int j_B \, d\omega}$$

$$= \frac{1}{x + d} \frac{\int \lambda j_B 2\pi\lambda \, d\lambda}{\int j_B 2\pi\lambda \, d\lambda}$$

$$\equiv \frac{\langle N \rangle}{x + d}$$

The same angle can be represented for the uniform exhaust profile as

$$\langle \tan \theta \rangle = \frac{\int_0^{\xi} j_B \frac{\lambda}{d} 2\pi\lambda \, d\lambda}{\int_0^{\xi} j_B 2\pi\lambda \, d\lambda}$$

$$= \frac{2\xi}{3d}$$

The focal point can be determined from the two preceding expressions as

$$d = \frac{x}{\frac{3}{2\xi} \langle N \rangle - 1}$$

The mean divergence angle and focal-point distance are included in the following table for the probe traces presented in figure 16. Integrated beam current and beam skew angles determined from the beam-contour maps are also presented. The skew angle was determined as shown in sketch (e). The values listed in the table represent a loss of less than 1 percent in thrust due to the combined beam offset or skew and spreading. The beam offset, however, results in a perpendicular thrust component of about 9 percent of the axial thrust.

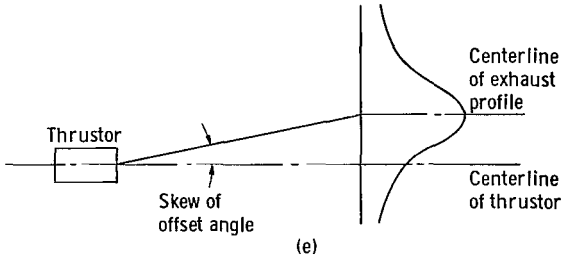

(e)

Shifting of the accelerator grid with respect to the screen grid was considered to be the principal contributing cause of the skew of the ion beam. The shifting could have

Ion-beam current (metered), J_B, amp	Beam current (integrated), J_B, amp	Skew angle, deg	Mean divergence angle, θ, deg	Focal point, cm
0.265	0.192	5.13	5.17	73.8
.496	.359	5.73	4.92	77.5
.752	.640	6.28	4.55	83.9
.975	1.034	5.73	6.25	60.8

been caused by (1) variations due to tolerances in the mechanical support structure for the grid insulators (2) alinement of thrustor modules and array within the mounting structure, (3) lack of rigidity in the method used for fastening the molybdenum grids to the stainless-steel supports, or (4) thermal expansion of grids and support structure as the operating temperature was approached. Grid spacings of 0.25 centimeter were used in the tests presented, and misalinement of up to 0.03 centimeter was possible. An improved design of the accelerator support structure could reduce this misalinement to 0.005 centimeter or less. The contours presented in figure 15 exhibit randomly skewed beams with major shifts in direction between runs due to relocation of the grids during maintenance and minor shifts in the support mechanism due to thermal effects. Distortion (lack of symmetry) of individual thrustor profiles was probably the result of thermal warping of the accelerator and screen grids due to impingement current and radiated cathode power.

The results of individual thrustor operation could be superimposed to provide the results of complete-array operation, as is somewhat apparent from the profiles of single- and multiple-thrustor operation. Single-probe traces best illustrate this point, however, and therefore the current to probe 8 during run 17 is presented in figure 17. The density contribution from thrustor 1 is negligible at this probe location. Superposition of the current probe trace obtained during single-thrustor operation on a trace of multiple-unit operation showed the two profiles are in good agreement.

Present laboratory thrustors will require some development from the standpoint of thermal stress relief and an improved support method for the accelerator grid in order to present a well-directed exhaust profile. Some small thrust skew will still be unavoidable, but the offset component of thrust on a large array due to the multiple random offsets will probably be quite small. Scheduling of power levels to various modules in the array could correct for this offset or thrust misalinement.

SUMMARY OF RESULTS

The following results were obtained from an investigation of the operation of an array of three 20-centimeter-diameter electron-bombardment ion thrustors with mercury as the propellant:

1. No appreciable steady-state interaction was observed between thrustors that could

be attributed to ion-chamber operating conditions or exhaust-beam density.

2. Slight thrustor interaction due to magnetic-field strength of adjacent thrustors was noticed at low values of magnetic field.

3. The proximity of operating thrustors did not cause additional accelerator impingement currents.

4. Neutralization of the array could be achieved with any or all of three immersed-type neutralizers that were connected to the exhaust beam by a plasma.

5. Interaction was present among neutralizers, inasmuch as the highest temperature neutralizer would supply most of the electrons. The potential level of the plasma was a function of the number of neutralizers used.

6. Beam spreading and thrust-vector misalinement were present and represent a small thrust loss and a perturbing force that may require compensation in flight arrays.

Lewis Research Center,
National Aeronautics and Space Administration,
Cleveland, Ohio, October 28, 1964.

APPENDIX A

SYMBOLS

A	Dushman's constant; theoretical value is 120 amp/(cm^2)($°K^2$)
a	solenoid radius, n
B	magnetic-field strength, gauss
C	perveance, amp/$v^{3/2}$
d	focal-point distance, n
$\mathscr{E}$	discharge chamber energy dissipated per beam ion, ev/ion
F	thrust, newtons
g	gravity constant, 9.81 m/sec^2
I	specific impulse, sec
J_A	accelerator impingement current, amp
J_B	ion-beam current, amp
j_B	ion-beam current density, amp/m^2
J_E	emission current, amp
J_F	filament heating current, amp
J_H	boiler heating current, amp
J_I	anode current, amp
J_M	magnetic-field current, amp
J_N	neutral propellant flow rate, equivalent amp
J_{NF}	neutralizer heating current, amp
J_{NE}	neutralizer emission current, amp
J_{NES}	space-charge-limited neutralizer emission current, amp
J_{SD}	screen-distributor current, amp
J_+	thrustor current, $J_B + J_A$, amp
$\sum J_+$	total thrustor current for array, $\sum J_+ = J_{+,1} + J_{+,2} + J_{+,3}$, amp
$\sum J_A$	total acceleration impingement current for array, $\sum J_A = J_{A,1} + J_{A,2} + J_{A,3}$, amp
$\sum J_B$	total thrustor beam current for array, $\sum J_B = J_{B,1} + J_{B,2} + J_{B,3}$, amp
K	Boltzmann's constant, 8.6×10^5 ev/°K
L	length of thrustor
ℓ	length of emitting neutralizer, m
$\dot{m}$	mass flow rate, kg/sec
m/q	mass-to-charge ratio, 2.08×10^{-6} kg/coulomb for Hg^{+1}
$\langle N \rangle$	$\left(\int 2\pi j_B \lambda^2 \, d\lambda\right) \Big/ \left(\int 2\pi j_B \lambda \, d\lambda\right)$
n	number of turns in thrustor solenoid
P_B	beam power, w
P_T	total power input to thrustor, w
R	ratio of net to total accelerating voltage, $V_I/(V_I + \lvert V_A \rvert)$
r	plasma sheath radius, m
T	neutralizer temperature, °K

V_A accelerator voltage, v

V_c collector voltage, v

V_F filament heating voltage, v

V_H boiler heating voltage, v

V_I net accelerating voltage, v

ΔV_I discharge voltage, v

V_M magnetic-field voltage, v

V_N neutralizer bias voltage, v

V_P plasma voltage, v

$\overline{v}$ average ion velocity, m/sec

x distance from accelerator surface to impingement probe plane, m

z solenoid cylindrical coordinate

α temperature coefficient of work function, ev/°K

β function of ratio of radius at any point to neutralizer radius

η_P thrustor power efficiency

η_U propellant-utilization efficiency

θ mean divergence angle, deg

λ distance from axis of thrustor to incremental area, m

μ permeability

ξ beam exhaust diameter at thrustor, m

ρ solenoid cylindrical coordinate

φ work function at T = 0° K, ev

ω area in ion density plane, m^2

Subscripts:

1, 2, 3 corresponding thrustor

APPENDIX B

CALCULATION OF MAGNETIC-FIELD-SUPERPOSITION EFFECTS

It is possible to array a group of ion thrustors in several ways. Thrustors utilizing magnetic-field windings for an N-unit array could be arranged with alternating polarity magnetic fields in a rectangular or equilateral triangle pattern as shown in the sketches (f) and (g). The magnetic field at adjacent thrustors may be determined either by using the Biot-Savart law or by defining the vector potential and performing the necessary curl operation. The latter method was used in reference 20 for a wide range of geometric variables for a finite solenoid. Each thrustor magnet winding may be approximated by the model shown in sketch (h).

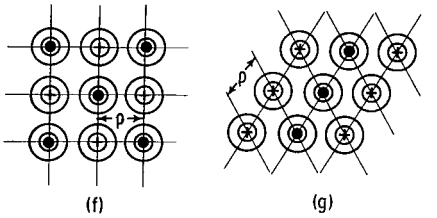

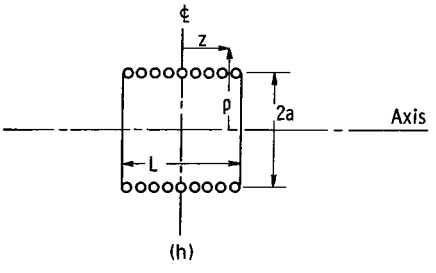

By using the plotted results of reference 20 for a typical thrustor geometry, it is possible to evaluate the field strength present at the screen of each thrustor. For $L/a = 2$ and a spacing between thrustors of 2.2 a (representative of the thrustors used in this report) the axial field B_z is presented in the table at the left for several values of radial position ρ at $2Z/L = 1$. By assuming an equal current and number of turns on each module and by using the superposition principle, the magnetic field can be determined for the center thrustor for the cases presented in sketches (f) and (g). For the first case, the magnetic field on the axis of the screen at the center thrustor for an N-module array can be expressed as the sum of the axial components of each solenoid as

ρ/a	$4B_z/\mu nJ_M$
0	1.79
2.2	-.08
3.1	-.03
≥ 4	$\sim$-.03

$$B_{z,\,axis} = B_{z,1} + B_{z,2} + B_{z,3} + B_{z,4} + \cdots + B_{z,N}$$

$$= B_{z,5} - 4B_{z,2} + 4B_{z,3} - \left(\frac{N}{2} - 4\right)B_z\left(\text{at } \frac{\rho}{a} > 4, \text{ same polarity as solenoid 5}\right)$$

$$+ \left(\frac{N}{2} - 5\right)B_z\left(\text{at } \frac{\rho}{a} > 4, \text{ opposite polarity as solenoid 5}\right)$$

$$= \left[1.79 - 4(0.08) + 4(-0.03) - \left(\frac{N}{2} - 4\right)(-0.03) + \left(\frac{N}{2} - 5\right)(-0.03)\right]\frac{\mu nJ_M}{4}$$

$$= 2.02 \times 4\mu nJ_M$$

The ratio of field strengths at the center thrustor is therefore

$$\frac{B_{z,\,total}}{B_{z,\,single}} = \frac{2.02}{1.79}$$

$$= 1.13$$

For the case illustrated in sketch (g),

$$B_z = \left[1.79 - 4(0.08) + 2(-0.08) - \left(\frac{N}{2} - 4\right)(-0.03) + \left(\frac{N}{2} - 3\right)(-0.03)\right]\frac{\mu n J_M}{4}$$

$$= 1.91 \times 4\mu n J_M$$

The ratio of field strengths is

$$\frac{B_{z,\,total}}{B_{z,\,single}} = \frac{1.91}{1.79}$$

$$= 1.07$$

It is therefore possible to increase the magnetic field at the screen from 7 to 13 percent by using the thrustor arrangements of sketches (g) and (f), respectively, compared with the single-thrustor field.

REFERENCES

1. Reader, Paul D., and Mickelsen, William R.: Experimental Systems Studies of Large Modules and Arrays of Electrostatic Thrustors. Paper 64-503, AIAA, 1964. (See also NASA TM X-52019, 1964.)

2. Reader, Paul D.: Experimental Performance of a 50-Centimeter Diameter Electron-Bombardment Ion Rocket. Paper 64-689, AIAA, 1964.

3. Stover, John B.: Electric Breakdown and Arcing in Experimental Ion Thrustor Systems. Paper 63057, AIAA, 1963.

4. Stover, John B.: Effects of Thrustor Arcing on Ion Rocket System Design. Paper 64-682, AIAA, 1964.

5. Pawlik, Eugene V., and Wenger, Norman C.: Performance Evaluation of a Mercury-Propellant Feed System for a Flight-Model Ion Engine. NASA TN D-1213, 1962.

6. Reader, Paul D.: Scale Effects on Ion Rocket Performance. ARS Jour., vol. 32, no. 5, May 1962, pp. 711-714.

7. Pawlik, Eugene V., and Nakanishi, Shigeo: Experimental Evaluation of Size Effects on Steady-State Control Properties of Electron-Bombardment Ion Thrustor. NASA TN D-2470, 1964.

8. Nakanishi, Shigeo, Pawlik, Eugene V., and Baur, Charles W.: Experimental Evaluation of Steady-State Control Properties of an Electron-Bombardment Ion Thrustor. NASA TN D-2171, 1964.

9. Kerslake, William R.: Accelerator Grid Tests on an Electron-Bombardment Ion Rocket. NASA TN D-1168, 1962.

10. Brunnée, Curt: Über die Ionenreflexion und Sekundarelektronenemission beim Auftreffen von Alkaliionen auf reine Molybdän-Oberflächen. (On the Ion Reflection and Secondary Electron Emission in the Collision of Alkali Ions with Pure Molybdenum Surfaces.) Zs. Phys., bd. 147, no. 2, 1957, pp. 161-183.

11. Kemp, Robert F., Sellen, J. M., Sr., and Pawlik, Eugene V.: Neutralization Tests on a Flight-Model Electron-Bombardment Ion Thrustor. NASA TN D-1733, 1963.

12. Kaufman, Harold R.: The Neutralization of Ion-Rocket Beams. NASA TN D-1055, 1961.

13. Kaufman, Harold R.: An Ion Rocket with an Electron-Bombardment Ion Source. NASA TN D-585, 1961.

14. Kerslake, William R.: Charge-Exchange Effects on the Accelerator Impingement of an Electron-Bombardment Ion Rocket. NASA TN D-1657, 1963.

15. Reader, Paul D.: An Electron-Bombardment Ion Rocket with a Permanent Magnet. Astronautics and Aerospace Eng., vol. 1, no. 9, Oct. 1963, p. 83. (See also Paper 63-031, AIAA, 1963.)

16. Spangenberg, Karl R.: Vacuum Tubes. McGraw-Hill Book Co., Inc., 1948.

17. Kohl, Walter H.: Materials and Techniques for Electron Tubes. Reinhold Pub. Corp., 1960.

18. Langmuir, Irving, and Compton, Karl T.: Electrical Discharges in Gases. II. Fundamental Phenomena in Electrical Discharges. Rev. Modern Phys., vol. 3, no. 2, Apr. 1931, pp. 191-257.

19. Mickelsen, William R., and Kaufman, Harold R.: Status of Electrostatic Thrustors for Space Propulsion. NASA TN D-2172, 1964.

20. Callaghan, Edmund E., and Maslen, Stephen H.: The Magnetic Field of a Finite Solenoid. NASA TN D-465, 1960.

TABLE I. - ION-CHAMBER PERFORMANCE OF CENTER THRUSTOR

[Interaction data for effects of discharge voltage and magnetic-field disturbances of outer thrustors on center thrustor. Net accelerating voltage, 4500 volts; accelerator voltage, -1500 volts.]

Thrustors operating	Discharge voltage, ΔV_I, v	Ion-beam current, J_B, amp	Accelerator current, J_A, amp	Anode current, J_I, amp	Emission current, J_E, amp	Magnetic-field current, J_M, amp	Discharge chamber energy, ϵ, ev/ion
Run 1							
1,2,3	30	0.229	0.001	6.2	7.4	11.0	779
1,2	30	.229	.001	6.1	7.4	11.0	766
2	30	.231	.001	6.1	7.4	11.0	760
1,2,3	40	0.249	0.001	5.4	5.0	11.0	827
1,2	40	.249	.001	5.5	5.0	11.0	844
2	40	.249	.001	5.1	5.0	11.0	779
1,2,3	50	0.259	0.001	4.8	3.9	11.0	877
1,2	50	.264	.001	4.8	3.8	11.0	860
2	50	.261	.001	4.8	3.8	11.0	869
1,2,3	60	0.254	0.001	3.9	2.7	11.0	862
1,2	60	.248	.002	3.9	2.8	11.0	880
2	60	.243	.001	3.8	2.6	11.0	873
1,2,3	70	0.261	0.001	4.4	2.8	11.0	1110
1,2	70	.261	.001	4.0	2.8	11.0	1003
2	70	.259	.001	4.0	2.8	11.0	1011
1,2,3	80	0.259	0.001	3.8	2.0	11.0	1093
1,2	80	.249	.001	3.8	2.1	11.0	1140
2	80	.249	.001	3.4	2.2	11.0	1012
1,2,3	90	0.264	0.001	4.0	2.2	11.0	1275
1,2	90	.259	.001	4.0	2.1	11.0	1300
2	90	.259	.001	3.9	2.1	11.0	1265
Run 2							
1,2,3	25	0.493	0.007	11.3	10.6	11.0	548
1,2	25	.498	.007	11.2	10.3	11.0	537
2	25	.493	.007	11.3	10.6	11.0	548
1,2,3	30	0.509	0.006	10.3	8.7	11.0	577
1,2	30	.518	.007	10.1	8.6	11.0	555
2	30	.509	.006	10.1	8.6	11.0	566
1,2,3	40	0.508	0.007	8.8	6.6	11.0	653
1,2	40	.533	.007	8.6	6.4	11.0	605
2	40	.519	.006	8.6	6.4	11.0	622
1,2,3	50	0.503	0.007	8.0	5.4	11.0	744
1,2	50	.489	.006	7.5	5.0	11.0	716
2	50	.489	.006	7.5	5.0	11.0	716
1,2,3	60	0.503	0.007	7.8	4.9	11.0	871
1,2	60	.503	.007	7.7	4.8	11.0	859
2	60	.503	.007	7.7	4.7	11.0	859
1,2,3	70	0.493	0.007	7.5	4.2	11.0	996
1,2	70	.493	.007	7.3	4.2	11.0	967
2	70	.493	.007	7.3	4.2	11.0	967
1,2,3	90	0.503	0.007	7.8	4.0	11.0	1304
1,2	90	.498	.007	7.6	4.0	11.0	1281
2	90	.493	.007	7.6	4.0	11.0	1299

Thrustors operating	Discharge voltage, ΔV_I, v	Ion-beam current, J_B, amp	Accelerator current, J_A, amp	Anode current, J_I, amp	Emission current, J_E, amp	Magnetic-field current, J_M, amp	Discharge chamber energy, ϵ, ev/ion
Run 3							
1,2,3	25	0.751	0.009	14.3	16.1	11.0	457
1,2	25	.731	.009	14.2	16.0	11.0	461
2	25	.721	.009	14.1	15.8	11.0	464
1,2,3	30	0.771	0.009	14.6	15.8	11.0	538
1,2	30	.791	.009	14.4	15.6	11.0	517
2	30	.781	.009	14.6	15.6	11.0	531
1,2,3	50	0.751	0.009	10.2	10.0	11.0	629
1,2	50	.737	.009	10.0	10.0	11.0	629
2	50	.721	.009	10.0	10.0	11.0	644
1,2,3	60	0.736	0.009	9.8	9.2	11.0	739
1,2	60	.721	.009	9.4	9.0	11.0	723
2	60	.711	.009	9.5	9.1	11.0	742
1,2,3	70	0.751	0.009	9.9	8.8	11.0	853
1,2	70	.746	.009	10.0	9.1	11.0	868
2	70	.736	.009	9.8	8.9	11.0	862
1,2,3	80	0.730	0.010	9.7	8.3	11.0	984
1,2	80	.710	.010	8.8	7.8	11.0	912
2	80	.700	.010	8.8	7.8	11.0	926
1,2,3	90	0.740	0.010	9.6	7.9	11.0	1077
1,2	90	.725	.010	9.4	7.8	11.0	1076
2	90	.710	.010	9.3	7.8	11.0	1089
Run 4							
1,2,3	25	0.983	0.022	24.6	27.0	11.0	600
1,2	25	.961	.019	24.4	26.8	11.0	609
2	25	.960	.020	24.2	26.4	11.0	606
1,2,3	30	1.003	0.017	19.6	19.6	11.0	556
1,2	30	.975	.015	19.2	19.6	11.0	560
2	30	.964	.016	19.0	19.6	11.0	560
1,2,3	40	0.966	0.014	15.6	15.0	11.0	605
1,2	40	.917	.013	15.4	15.2	11.0	633
2	40	.926	.014	15.4	15.0	11.0	626
1,2,3	50	0.984	0.016	16.0	15.1	11.0	763
1,2	50	.970	.015	15.7	14.8	11.0	758
2	50	.965	.016	15.7	14.7	11.0	761
1,2,3	60	1.003	0.017	16.0	13.6	11.0	897
1,2	60	.963	.017	15.4	13.8	11.0	897
2	60	.970	.020	15.2	13.6	11.0	879
1,2,3	80	0.987	0.023	15.6	12.6	11.0	1184
1,2	80	.942	.018	15.0	12.5	11.0	1189
2	80	.951	.019	15.0	12.6	11.0	1179

TABLE I. - Concluded. ION-CHAMBER PERFORMANCE OF CENTER THRUSTOR

[Interaction data for effects of discharge voltage and magnetic-field disturbances of outer thrustors on center thrustor. Net accelerating voltage, 4500 volts; accelerator voltage, -1500 volts.]

Thrustors operating	Discharge voltage, ΔV_I, v	Ion-beam current, J_B, amp	Accelerator current, J_A, amp	Anode current, J_I, amp	Emission current J_E, amp	Magnetic-field current, J_M, amp	Discharge chamber energy, ϵ, ev/ion
Run 5							
1,2,3	50	0.249	0.001	10.4	9.6	5.0	2040
1,2	50	.274	.001	10.8	10.0	5.0	1922
2	50	.279	.001	10.4	9.8	5.0	1822
1,2,3	50	0.259	0.001	6.0	5.0	7.0	1110
1,2	51	.259	.001	5.8	5.0	7.0	1092
2	51	.249	.001	5.8	5.0	7.0	1137
1,2,3	50	0.249	0.001	4.2	3.3	9.0	794
1,2	50	.259	.001	4.0	3.0	9.0	722
2	50	.249	.001	4.0	3.0	9.0	754
1,2,3	50	0.264	0.001	4.1	3.1	11.0	728
1,2	50	.259	.001	4.0	3.1	11.0	722
2	50	.264	.001	4.0	3.1	11.0	728
1,2,3	50	0.269	0.001	4.1	3.1	13.0	712
1,2	51	.264	.001	4.0	3.0	13.0	722
2	51	.249	.001	3.8	3.0	13.0	727
1,2,3	50	0.274	0.001	4.0	3.0	15.0	679
1,2	50	.249	.001	3.8	3.0	15.0	713
2	50	.229	.001	3.6	2.9	15.0	736
1,2,3	50	0.254	0.001	3.8	3.0	17.0	699
1,2	50	.249	.001	3.9	3.0	17.0	733
2	50	.259	.001	3.9	3.0	17.0	704
Run 6							
1,2,3	50	0.497	0.003	20.5	18.4	5.0	2020
1,2	50	.517	.003	21.7	19.5	5.0	1982
2	50	.546	.004	21.0	19.1	5.0	1875
1,2,3	50	0.502	0.003	10.4	8.8	9.0	986
1,2	50	.482	.003	10.0	8.7	9.0	988
2	50	.477	.003	10.0	8.6	9.0	997
1,2,3	50	0.502	0.003	9.0	7.4	11.0	847
1,2	50	.507	.003	8.6	7.1	11.0	798
2	50	.507	.003	8.3	6.9	11.0	768
1,2,3	50	0.507	0.003	9.2	7.4	13.0	857
1,2	50	.507	.003	8.6	7.0	13.0	798
2	50	.487	.003	8.9	7.7	13.0	863
1,2,3	50	0.497	0.003	8.6	6.9	15.0	815
1,2	50	.497	.003	8.2	7.0	15.0	775
2	50	.502	.003	8.2	6.9	15.0	767
1,2,3	50	0.511	0.004	7.6	6.0	17.0	693
1,2	50	.501	.004	7.4	6.0	17.0	688
2	50	.491	.004	7.4	6.0	17.0	704
Run 7							
1,2,3	50	0.739	0.008	20.5	17.0	7.0	1337
1,2	50	.729	.009	20.2	17.8	7.0	1335
2	50	.719	.008	20.2	17.6	7.0	1354
1,2,3	50	0.740	0.009	13.4	10.2	9.0	855
1,2	50	.760	.008	13.2	10.4	9.0	819
2	50	.760	.008	13.1	10.3	9.0	811
1,2,3	50	0.752	0.008	12.8	9.7	11.0	801
1,2	50	.777	.008	12.6	9.8	11.0	754
2	50	.762	.008	12.5	9.6	11.0	770
1,2,3	50	0.746	0.008	11.2	8.1	13.0	701
1,2	50	.756	.008	11.2	8.1	13.0	691
2	50	.756	.008	10.9	8.5	13.0	671
1,2,3	50	0.760	0.009	11.0	8.1	15.0	674
1,2	50	.750	.009	11.0	8.4	15.0	683
2	50	.740	.010	10.7	8.3	15.0	673
1,2,3	50	0.728	0.010	10.3	7.4	17.0	657
1,2	50	.723	.011	10.0	7.8	17.0	642
2	50	.688	.010	9.6	7.5	17.0	647
Run 8							
1,2,3	50	0.985	0.015	26.6	24.4	7.0	1300
1,2	50	1.025	.015	27.0	25.0	7.0	1268
2	50	1.063	.017	27.0	25.0	7.0	1222
1,2,3	50	0.966	0.014	18.6	16.4	9.0	912
1,2	50	.946	.014	18.4	17.2	9.0	919
2	50	1.024	.021	18.8	17.4	9.0	868
1,2,3	50	0.987	0.023	15.6	14.0	15.0	740
1,2	50	.997	.023	15.7	14.6	15.0	738
2	50	1.005	.025	15.8	14.6	15.0	736
1,2,3	50	0.972	0.028	14.2	12.2	13.0	679
1,2	50	.962	.028	14.0	13.0	13.0	676
2	50	.972	.028	14.0	13.0	13.0	669
1,2,3	50	0.966	0.034	13.4	11.6	15.0	642
1,2	50	.964	.036	13.0	12.4	15.0	622
2	50	.965	.035	13.0	12.4	15.0	622
1,2,3	50	0.968	0.032	13.0	11.2	17.0	620
1,2	50	.965	.035	12.8	12.4	17.0	612
2	50	.974	.036	12.8	12.4	17.0	606

TABLE II. - ACCELERATOR PERFORMANCE OF CENTER THRUSTOR

[Interaction data for effects of outer thrustor operation on center thrustor. Discharge voltage, 50 volts; magnetic-field current, 11 amperes (magnetic-field strength, about 14.5 gauss).]

Thrustors operating	Anode voltage, V_I, v	Accelerator voltage, V_A, v	Ion-beam current, J_B, amp	Accelerator current, J_A, amp	Anode current, J_I, amp	Emission current, J_E, amp
			Run 9a			
1,2,3	5400	-1360	0.250	0.0018	2.2	1.7
	4800	-1200	.251	.0019	2.3	1.8
	4400	-1100	.255	.0019	2.5	1.9
	4000	-1000	.255	.0018	2.7	2.1
	3600	-900	.252	.0018	2.9	2.3
	3200	-800	.247	.0017	2.9	2.4
	2800	-700	.255	.0019	3.4	2.7
	2600	-650	.250	.0027	3.4	2.8
	2500	-625	.251	.0030	----	----
	2400	-600	.250	.0051	----	----
	2300	-580	.249	.0070	----	----
	2200	-550	.245	.0100	----	----
			Run 9b			
2	4000	-1000	0.252	0.0018	2.4	1.8
	2800	-700	.250	.0017	3.0	2.4
	2600	-650	.250	.0022	3.2	2.5
	2400	-615	.255	.0033	3.3	2.5
	2300	-575	.249	.0047	3.3	2.5
	2200	-545	.258	.0093	3.5	2.6
			Run 10a			
1,2,3	4500	-1500	0.478	0.0023	8.8	7.1
	4000	-1340	.483	.0021	9.0	7.1
	3700	-1240	.483	.0024	10.5	8.6
	3600	-1200	.521	.0044	10.6	8.6
	3500	-1150	.503	.0054	10.9	8.8
	3400	-1120	.502	.0079	14.5	12.9
	3300	-1100	.515	.0150	15.5	13.5
	3200	-1060	.464	.0560	14.6	13.0
			Run 10b			
2	6000	-2000	0.513	0.0020	10.6	9.3
	4500	-1500	.483	.0019	10.7	8.4
	4000	-1330	.493	.0027	11.5	11.2
	3700	-1250	.487	.0033	12.6	11.5
	3600	-1200	.499	.0064	15.3	14.8
	3500	-1150	.502	.0083	15.4	14.8
	3400	-1120	.496	.0088	15.3	14.8
	3300	-1105	.471	.0092	15.1	14.6
	3200	-1060	.490	.0147	16.5	16.4
	3100	-1030	.473	.0371	16.7	16.5

TABLE III. - NEUTRALIZATION DATA FOR SINGLE- AND MULTIPLE-THRUSTOR OPERATION

[Net accelerating voltage, 4500 volts; accelerator voltage, -1500 volts; discharge voltage, 50 volts; magnetic-field current, 11 amperes (magnetic-field strength, about 14.5 gauss); neutralizer bias voltage, 20 volts.]

Thrustor			Neutralizer			Collector to neutralizer potential difference, $V_c - V_N$, v
1	2	3	1	2	3	
Ion-beam current, J_B, amp			Neutralizer emission current, J_{NE}, amp			
Run 11						
0.250	0	0	0.250	0	0	3
0	.243	0	0	.243	0	3
0	.285	0	0	.283	0	4
0	.510	0	0	.480	0	4
0	.830	0	0	.820	0	6
0	0	.260	0	0	.260	3
Run 12						
0.270	0.240	0	0.255	0.230	0	4
0	.250	.255	0	.240	.255	4
0	.255	.245	0	0	.480	7 to 8
0	.260	.255	0	.310	.190	6
0	.250	.245	0	.490	0	9
.250	0	.265	.280	0	.220	4 to 5
.245	0	.260	.500	0	0	6 to 8
.250	0	.260	0	0	.490	6 to 8
.255	0	.260	.350	0	.150	6 to 7
Run 13						
0.275	0.255	0.265	0.260	0.260	0.240	4
.255	.250	.250	.730	0	0	11
.240	.255	.255	0	.725	0	11 to 14
.235	.250	.253	0	0	.780	9 to 10
.245	.245	.250	.340	.390	0	7
.255	.265	.265	0	.390	.360	7
.245	.250	.245	0	.490	.230	9
.250	.255	.255	0	.280	.460	7 to 8
.240	.245	.250	.270	.380	.120	6
.245	.250	.250	.120	.480	.130	8 to 9
.245	.245	.260	.130	.400	.200	7 to 8
.245	.250	.250	.210	.420	.110	7 to 8
Run 14						
0.510	0	0.530	0.480	0	0.530	4 to 5
.520	0	.515	.980	0	0	9 to 10
.250	0	.520	0	0	1.010	8
.520	0	.510	.780	0	.200	8 to 9
.530	.480	.500	.450	.550	.470	7 to 8
.510	.590	.580	1.150	.230	.230	12 to 13
.480	.520	.480	.220	.900	.180	10 to 13
.486	.500	.500	.300	.300	.820	8 to 10

TABLE IV. - THRUSTOR OPERATION DURING BEAM-DENSITY SURVEY

[Net accelerating voltage, 4500 volts; accelerator voltage, -1500 volts; discharge voltage, 50 volts; magnetic-field current, 11 amperes (magnetic-field strength, about 14.5 gauss).]

Thrustors operating	Ion-beam current, J_B, amp	Accelerator impingement current, J_A, amp	Anode current J_I, amp	Emission current, J_E, amp	Thrustor	Propellant utilization, efficiency, η_u	Thrust, F, newtons	Specific impulse, I, sec
				Run 15				
1	0.262	0.0024	3.8	3.4	1	0.90	0.036	6030
2	.265	.0018	3.6	3.0	2	.85	.036	5700
3	.253	.0013	3.6	3.0	3	.85	.035	5700
1,2,3	0.258	0.0022	3.9	3.4	1	0.85	0.103	5700
	.249	.0014	4.3	3.6	2			
	.248	.0015	4.0	3.1	3			
				Run 16				
1	0.495	0.0048	8.1	6.9	1	0.85	0.068	5700
2	.496	.0040	8.9	7.0	2	.85	.068	5700
3	.495	.0052	6.2	5.1	3	.75	.068	5020
1,2,3	0.495	0.0053	8.2	6.9	1	0.85	0.204	5700
	.497	.0025	8.4	7.0	2			
	.495	.0045	7.7	6.4	3			
				Run 17				
1	0.736	0.0250	12.3	9.3	1	0.80	0.100	5360
2	.752	.0083	11.6	11.3	2	.85	.103	5700
3	.724	.0026	10.2	10.0	3	.80	.099	5360
1,2,3	0.713	0.0170	12.6	9.4	1	0.80	0.293	5360
	.731	.0090	10.0	9.9	2			
	.700	.0025	10.5	10.3	3			
				Run 18				
1	0.952	0.0480	21.8	17.5	1	0.90	0.130	6030
2	.975	.0200	15.8	14.5	2	.85	.133	5700
3	.934	.0660	14.7	14.4	3	.85	.128	5700
1,2,3	0.963	0.0470	22.5	18.2	1	0.85	0.393	5700
	.973	.0170	13.9	12.0	2			
	.934	.0560	15.0	14.8	3			

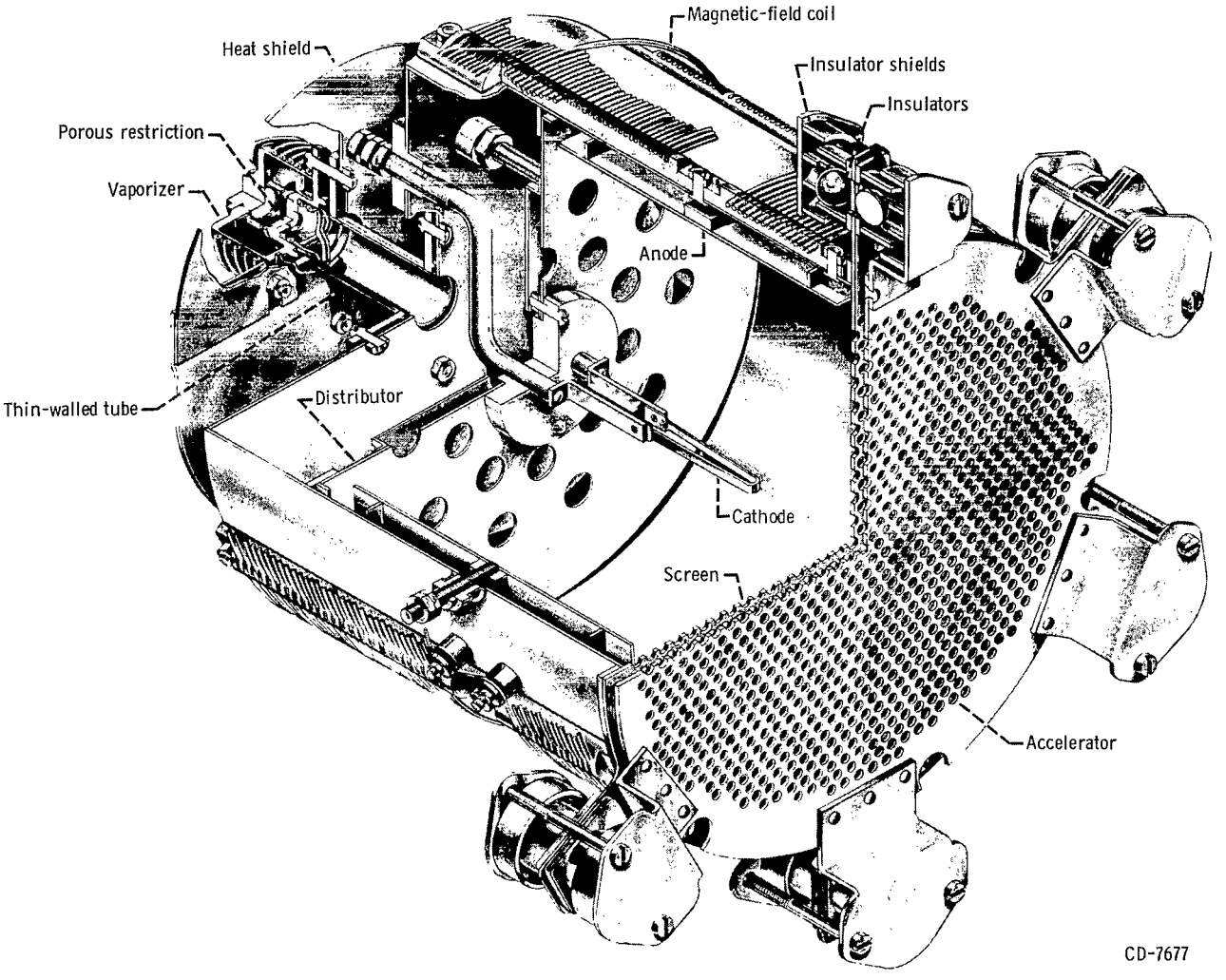

Figure 1. - Cutaway drawing of 20-centimeter-diameter electron-bombardment ion thrustor.

Figure 2. - Installation showing three-thrustor array in thrustor compartment.

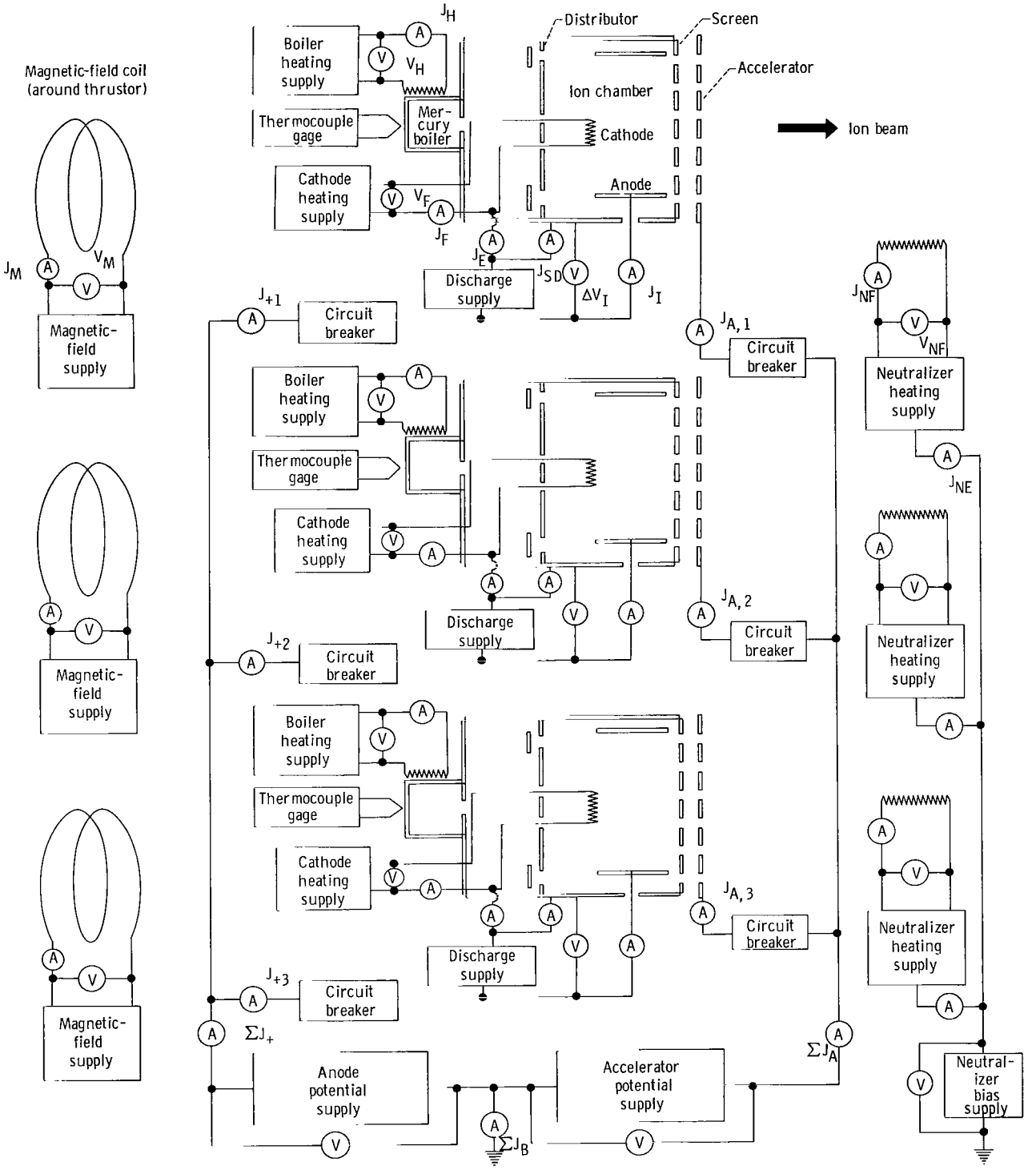

Figure 3. - Wiring diagram for array of three ion thrustors.

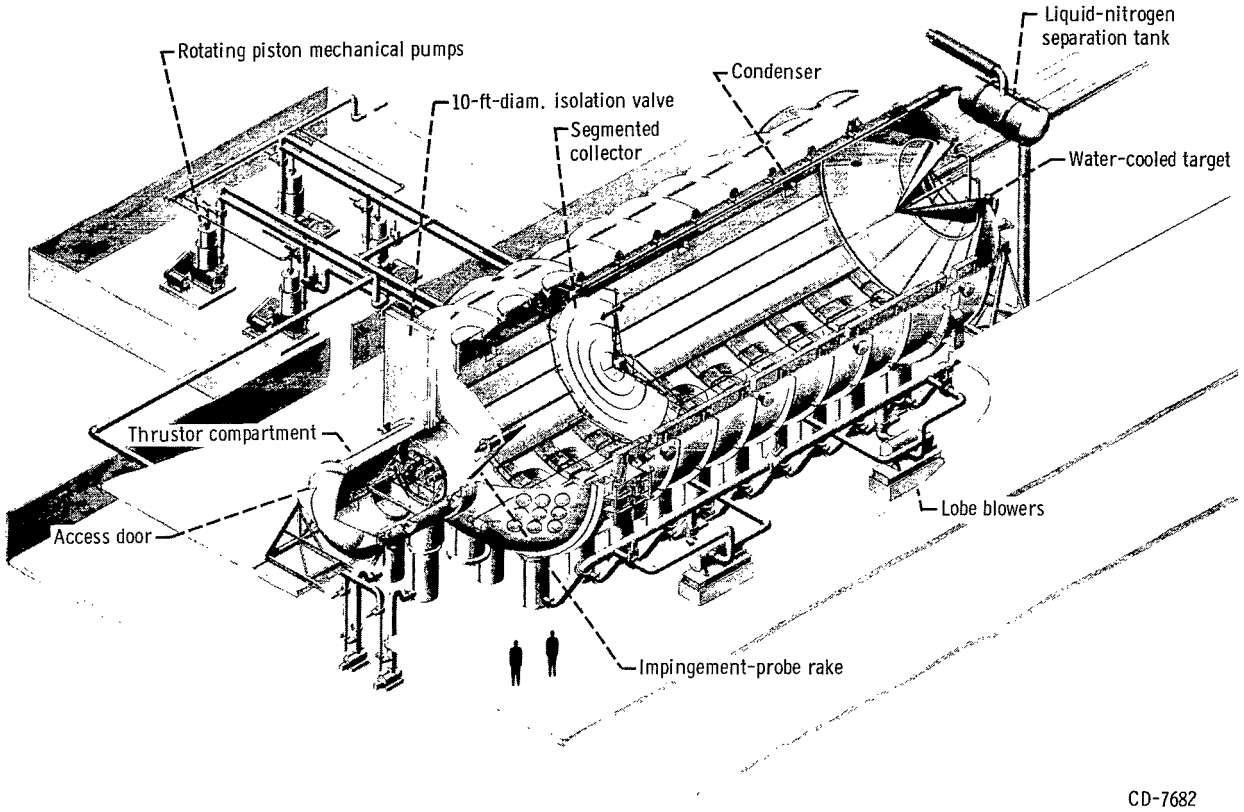

Figure 4. - Cutaway view of vacuum facility.

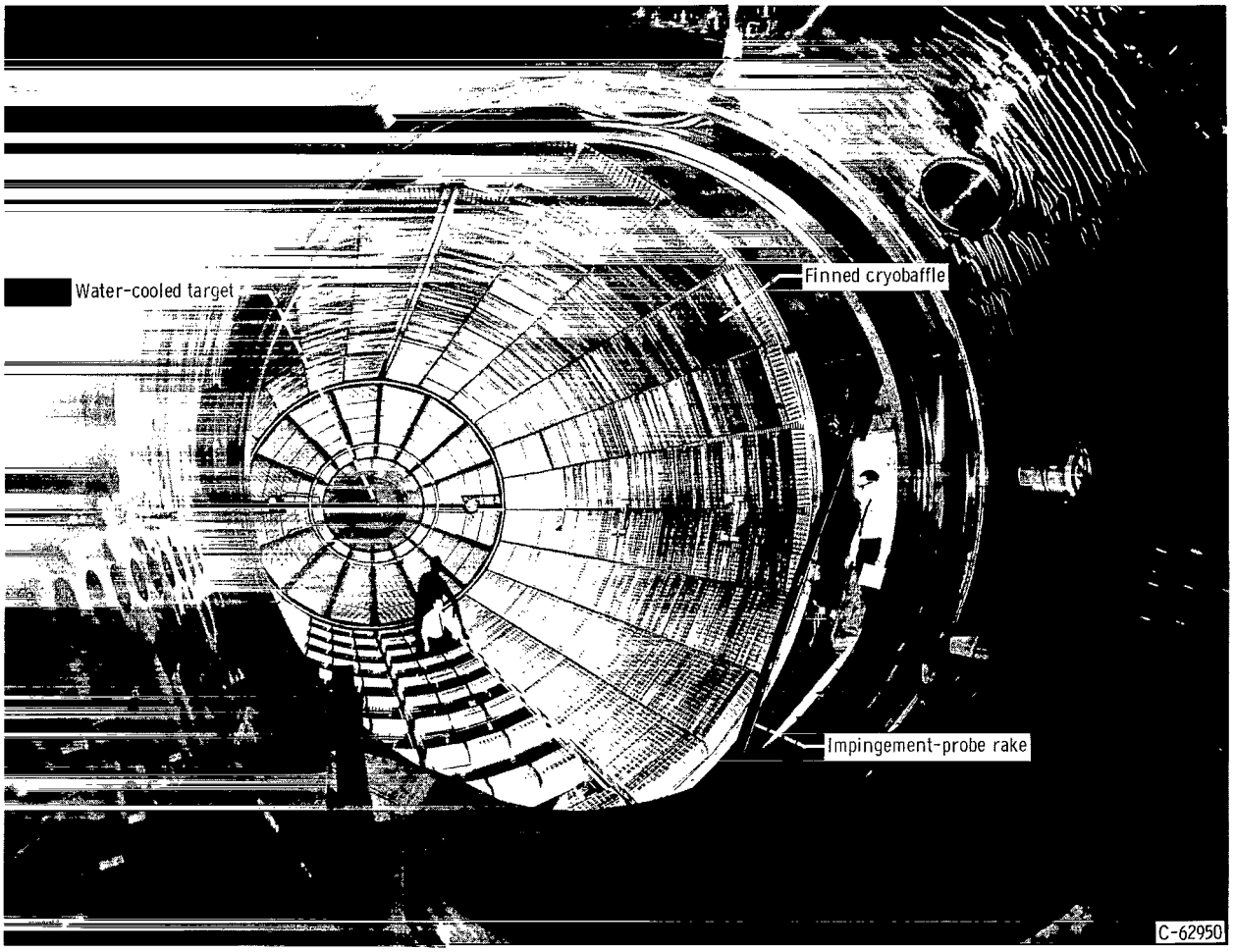

Figure 5. - Vacuum tank interior before installation of ion-beam collector and thrustor array.

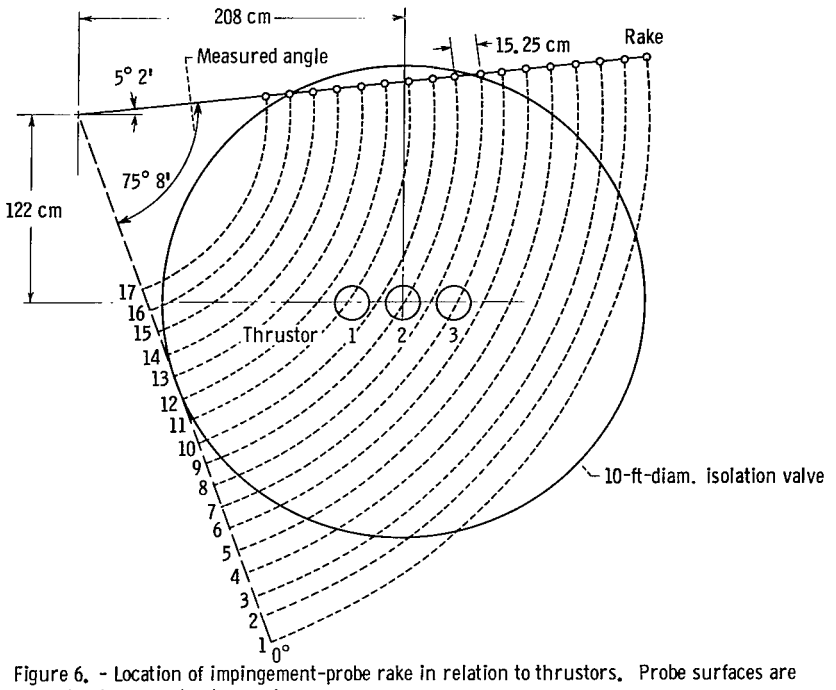

Figure 6. - Location of impingement-probe rake in relation to thrustors. Probe surfaces are 1 meter from accelerator surfaces.

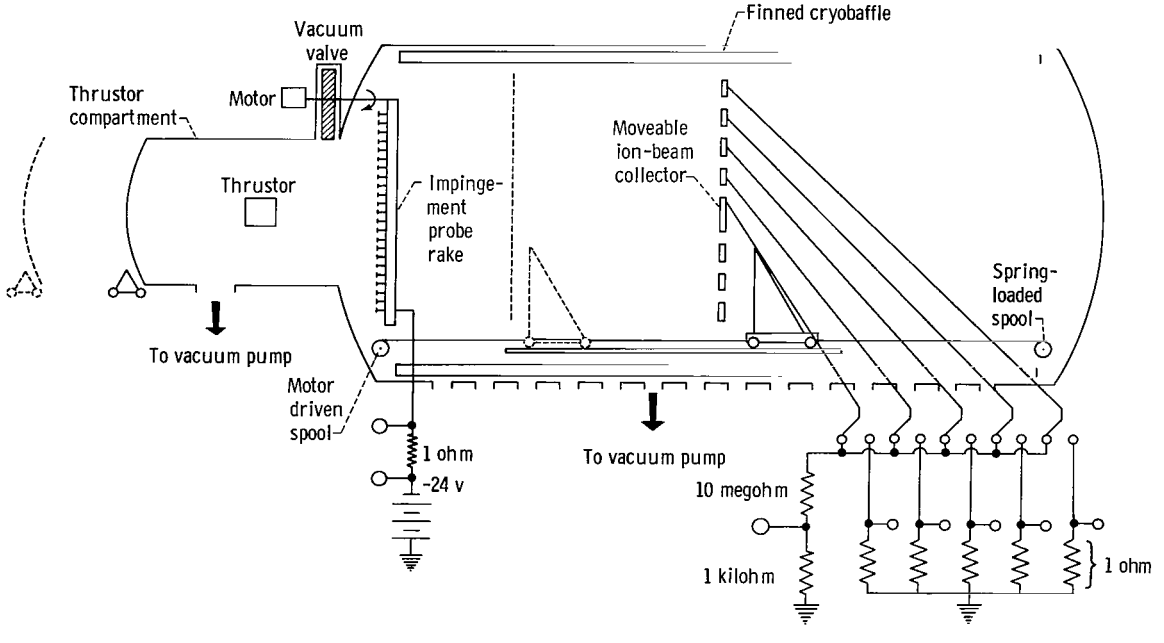

Figure 7. - Schematic diagram of vacuum chamber and beam instrumentation.

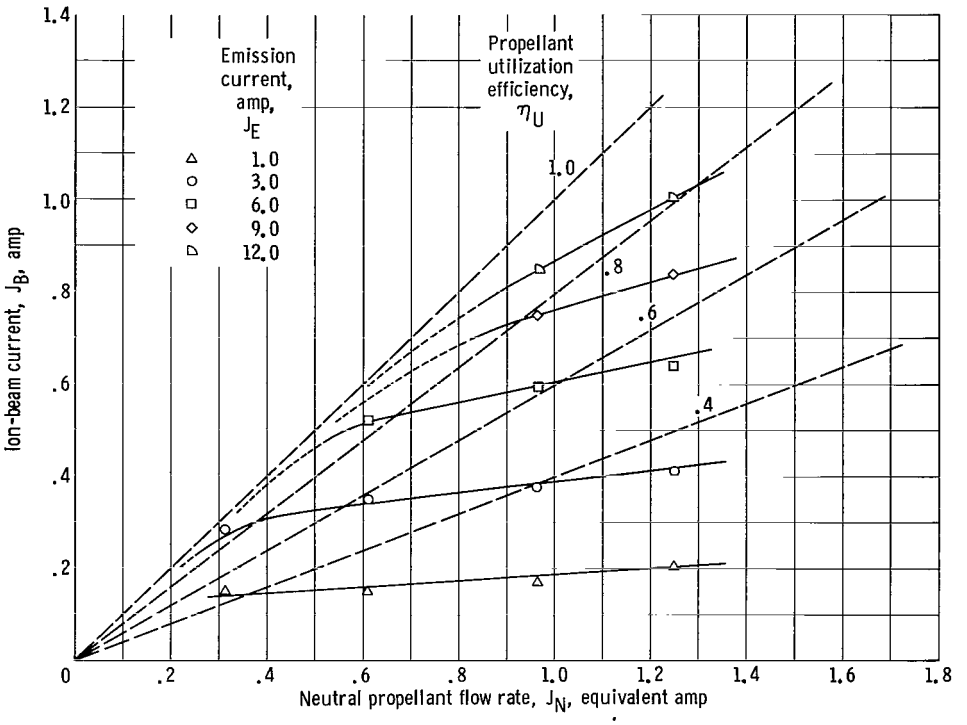

Figure 8. - Ion-beam - propellant flow characteristics at constant emission (ref. 7). Net accelerating voltage, 4000 volts; accelerator voltage, -1000 volts; discharge voltage, 50 volts; magnetic-field strength, 17.2 gauss.

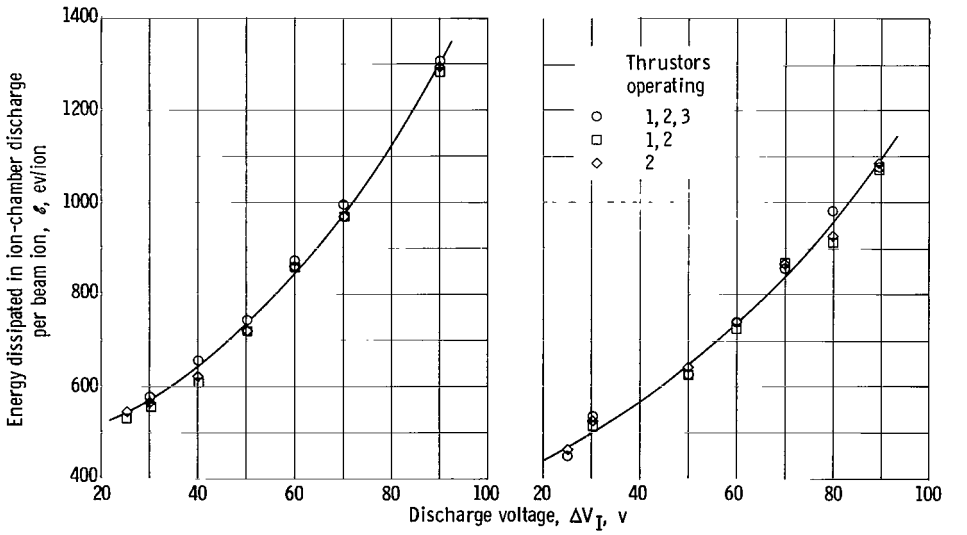

(a) Ion-beam current per operating thrustor, 0.50 ampere.

(b) Ion-beam current per operating thrustor, 0.75 ampere.

Figure 9. - Energy dissipated in ion chamber of center thrustor as function of its discharge voltage with thrustors 1, 2, and 3 operating. Net accelerating voltage, 4500 volts; accelerator voltage, -1500 volts; discharge voltage, 50 volts on thrustors 1 and 3 when operating, otherwise zero; magnetic-field strength, 14.5 gauss.

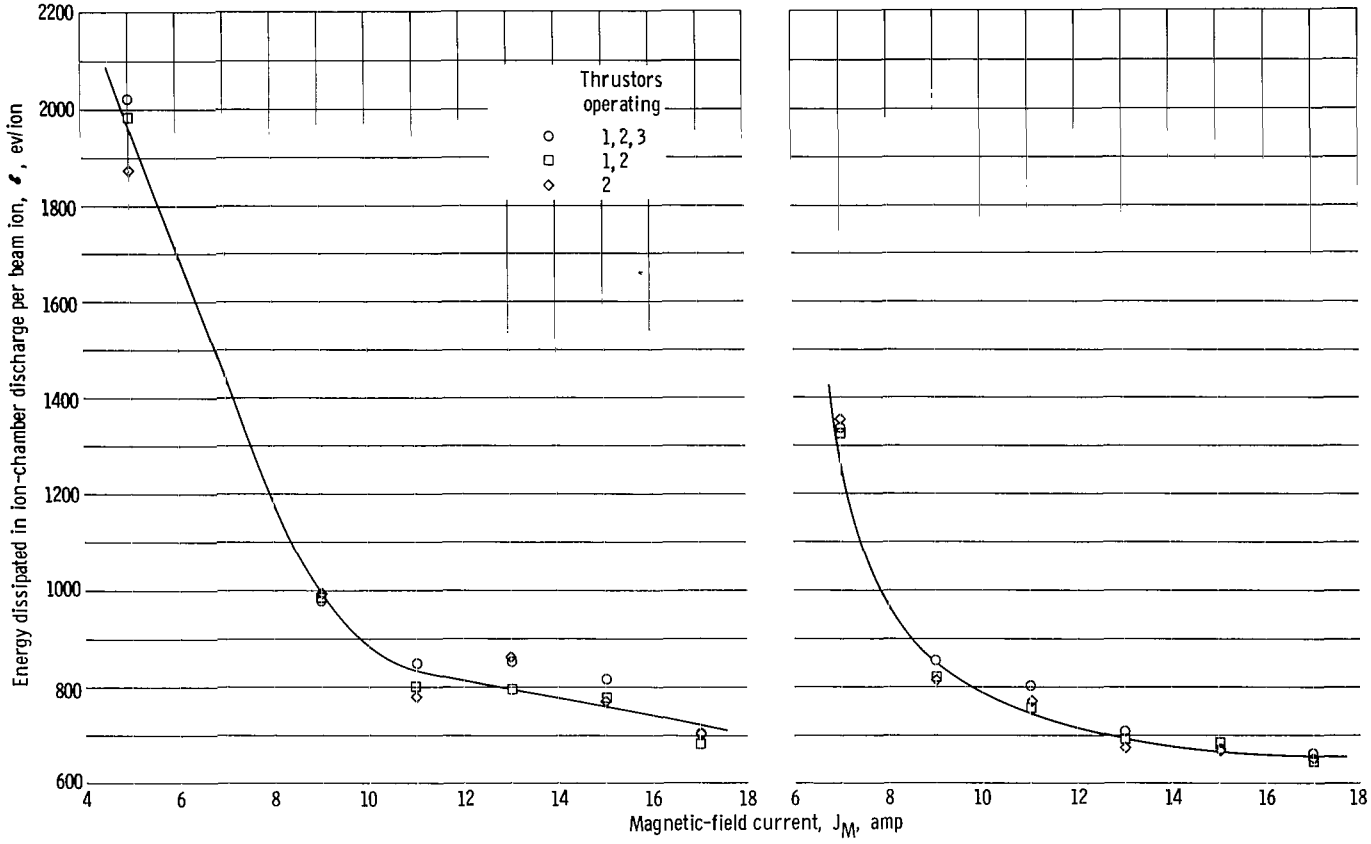

(a) Ion-beam current per operating thrustor, 0.50 ampere.

(b) Ion-beam current per operating thrustor, 0.75 ampere.

Figure 10. - Energy dissipated in ion chamber of center thrustor as function of its magnetic field with thrustors 1, 2, and 3 operating. Net accelerating voltage, 4500 volts; accelerator voltage, -1500 volts; discharge voltage, 50 volts for all thrustors; magnetic-field current, 11 amperes on thrustors 1 and 3 when operating, otherwise zero.

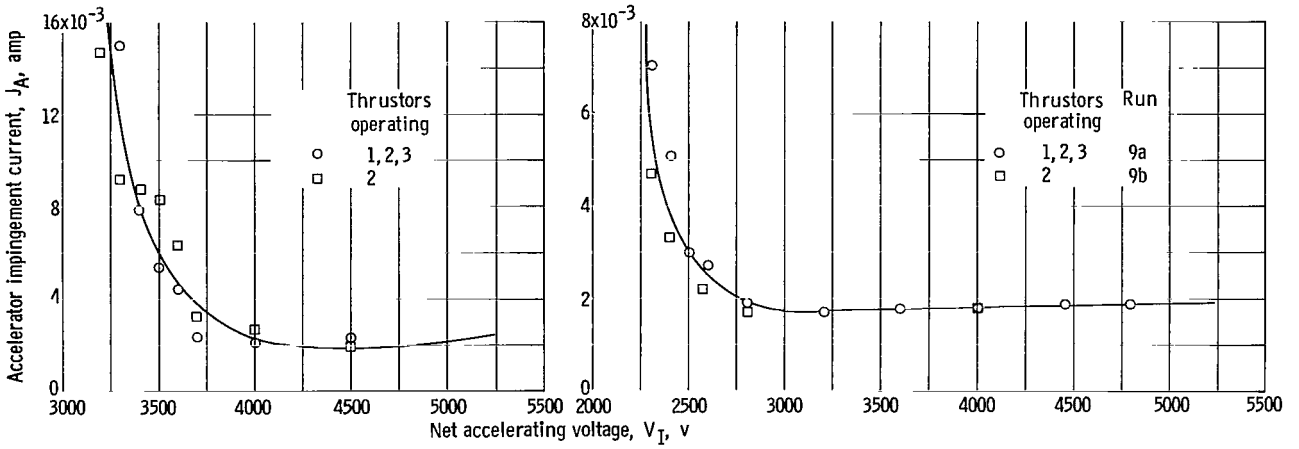

(a) Ion-beam current for operating thrustor, 0.50 ampere.

(b) Ion-beam current for operating thrustor, 0.25 ampere.

Figure 11. - Accelerator impingement current for center thrustor as function of net accelerating voltage for single- and three-thrustor operation. Discharge voltage, 50 volts; magnetic-field strength, 14.5 gauss.

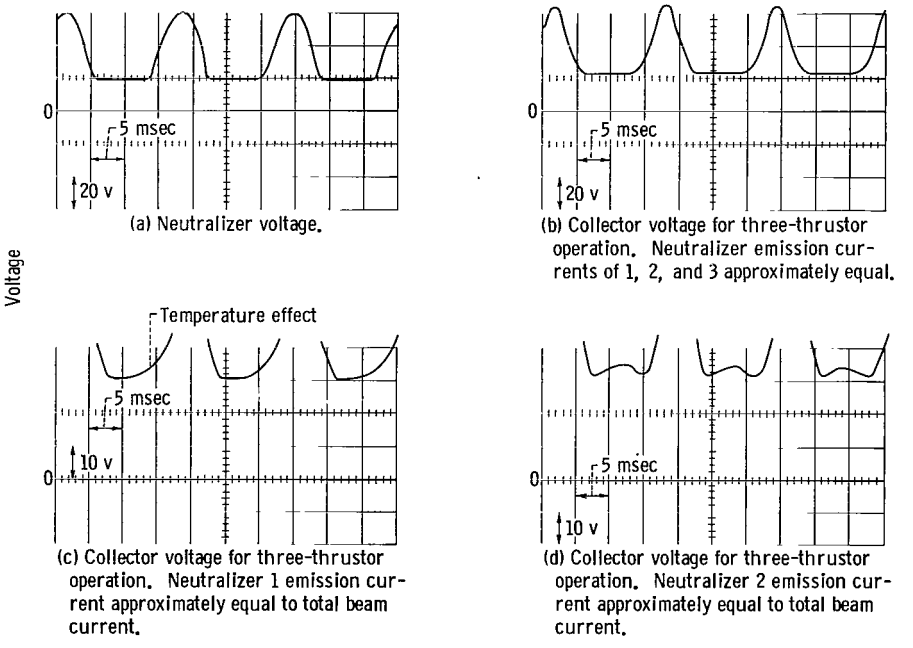

(a) Neutralizer voltage.

(b) Collector voltage for three-thrustor operation. Neutralizer emission currents of 1, 2, and 3 approximately equal.

(c) Collector voltage for three-thrustor operation. Neutralizer 1 emission current approximately equal to total beam current.

(d) Collector voltage for three-thrustor operation. Neutralizer 2 emission current approximately equal to total beam current.

Figure 12. - Typical waveforms for neutralizer and collector voltage.

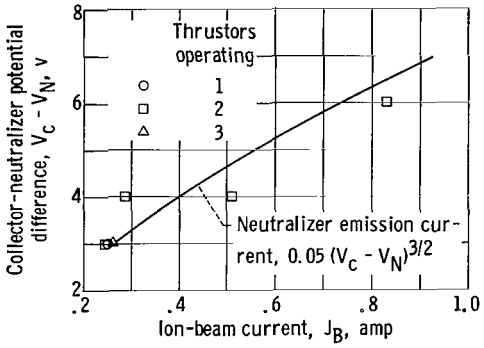

Figure 13. - Collector-neutralizer potential difference as function of ion-beam current for single-thrustor operation. Net accelerating voltage, 4500 volts; accelerator voltage, -1500 volts; discharge voltage, 50 volts; magnetic-field current, 11.0 amperes.

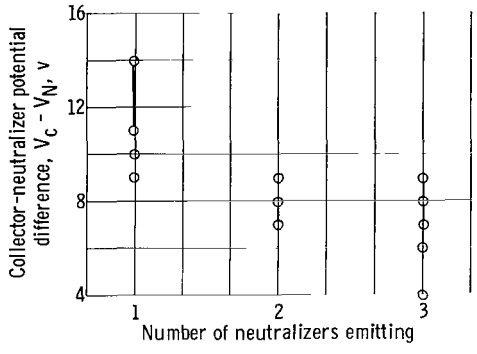

Figure 14. - Collector-neutralizer potential difference against number of neutralizers emitting during three-thrustor operation. Net accelerating voltage, 4500 volts; accelerator voltage, -1500 volts; discharge voltage, 50 volts; magnetic-field current, 11.0 amperes.

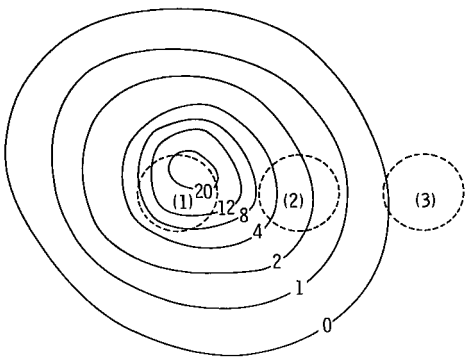

Thrustor 1 operating. Total thrustor beam current, 0.253 ampere. Run 15c.

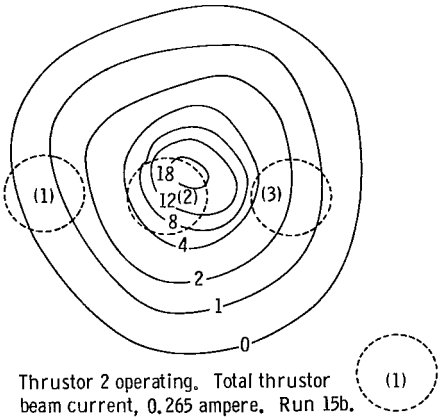

Thrustor 2 operating. Total thrustor beam current, 0.265 ampere. Run 15b.

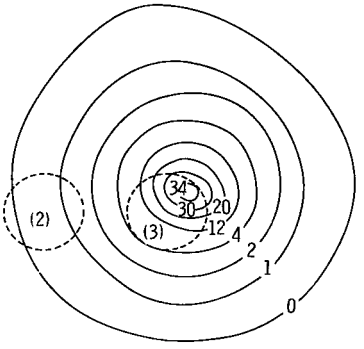

Thrustor 3 operating. Total thrustor beam current, 0.262 ampere. Run 15a.

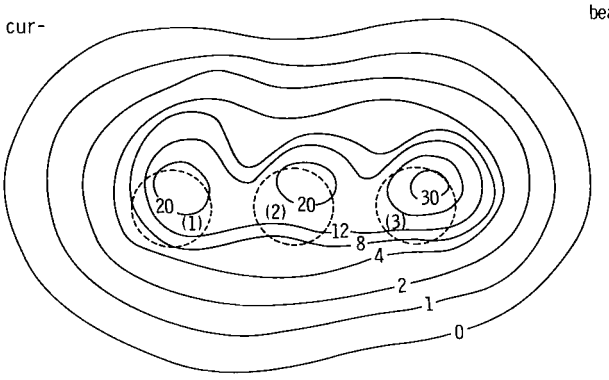

Thrustors 1, 2, and 3 operating. Total thrustor beam current, 0.755 ampere. Run 15d.

(a) Thrustors operating near 0.25 ampere beam current. Relative beam intensity numbers on contours correspond to 15 microamperes per unit.

Figure 15. - Ion-beam contour maps for various modes of operation.

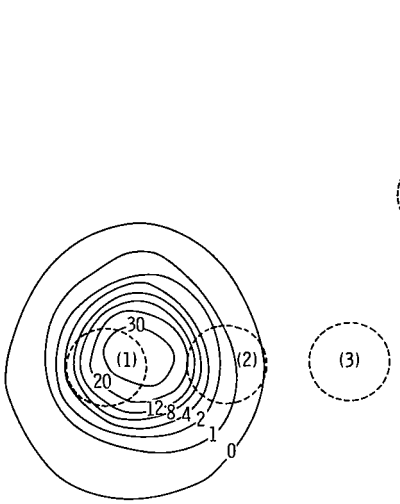

Thrustor 1 operating. Total thrustor beam current, 0.445 ampere. Run 16c.

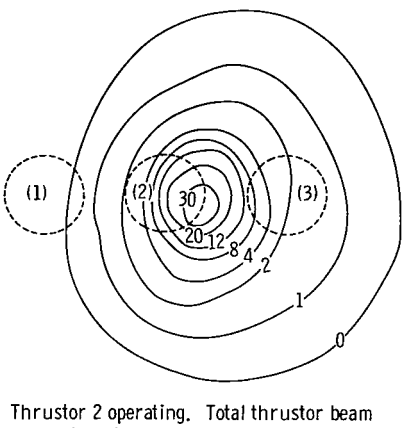

Thrustor 2 operating. Total thrustor beam current, 0.496 ampere. Run 16b.

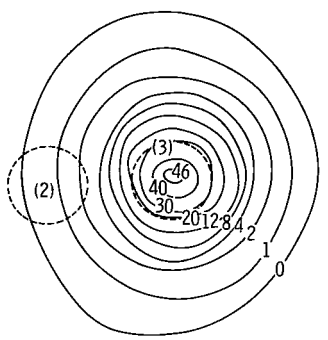

Thrustor 3 operating. Total thrustor beam current, 0.495 ampere. Run 16a.

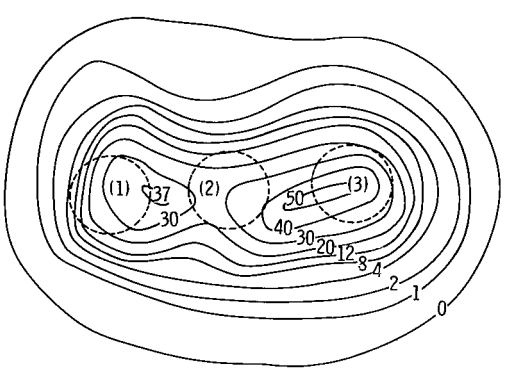

Thrustors 1, 2, and 3 operating. Total thrustor beam current, 1.487 amperes. Run 16d.

(b) Thrustors operating near 0.50 ampere beam current. Relative beam intensity numbers on contours correspond to 20 microamperes per unit.

Figure 15. - Continued. Ion-beam contour maps for various modes of operation.

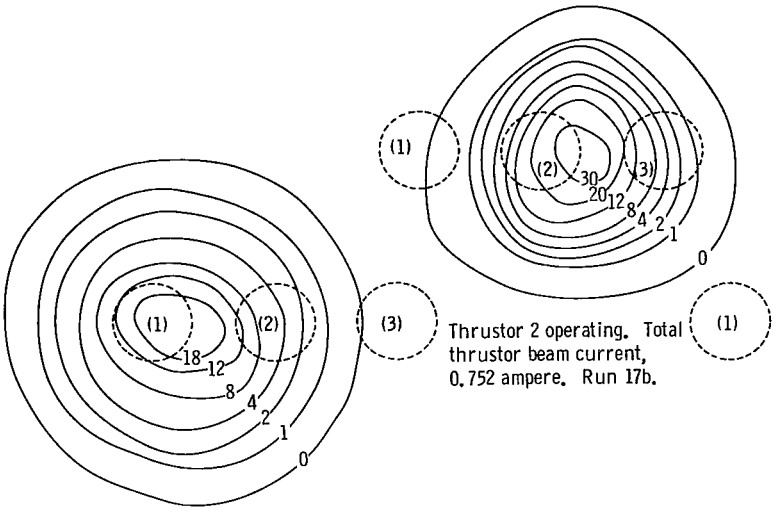

Thrustor 2 operating. Total thrustor beam current, 0.752 ampere. Run 17b.

Thrustor 1 operating. Total thrustor beam current, 0.724 ampere. Run 17c.

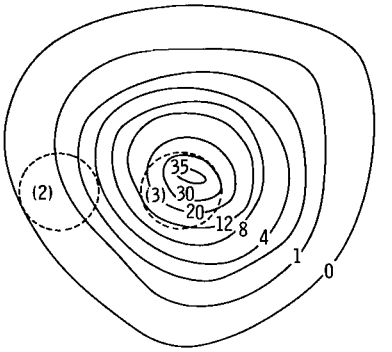

Thrustor 3 operating. Total thrustor beam current, 0.736 ampere. Run 17a.

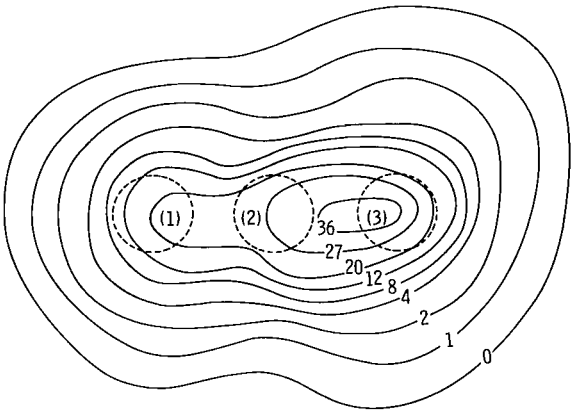

Thrustors 1, 2, and 3 operating. Total thrustor beam current, 2.144 amperes. Run 17d.

(c) Thrustors operating near 0.75 ampere beam current. Relative beam intensity numbers on contours correspond to 30 microamperes per unit.

Figure 15. - Continued. Ion-beam contour maps for various modes of operation.

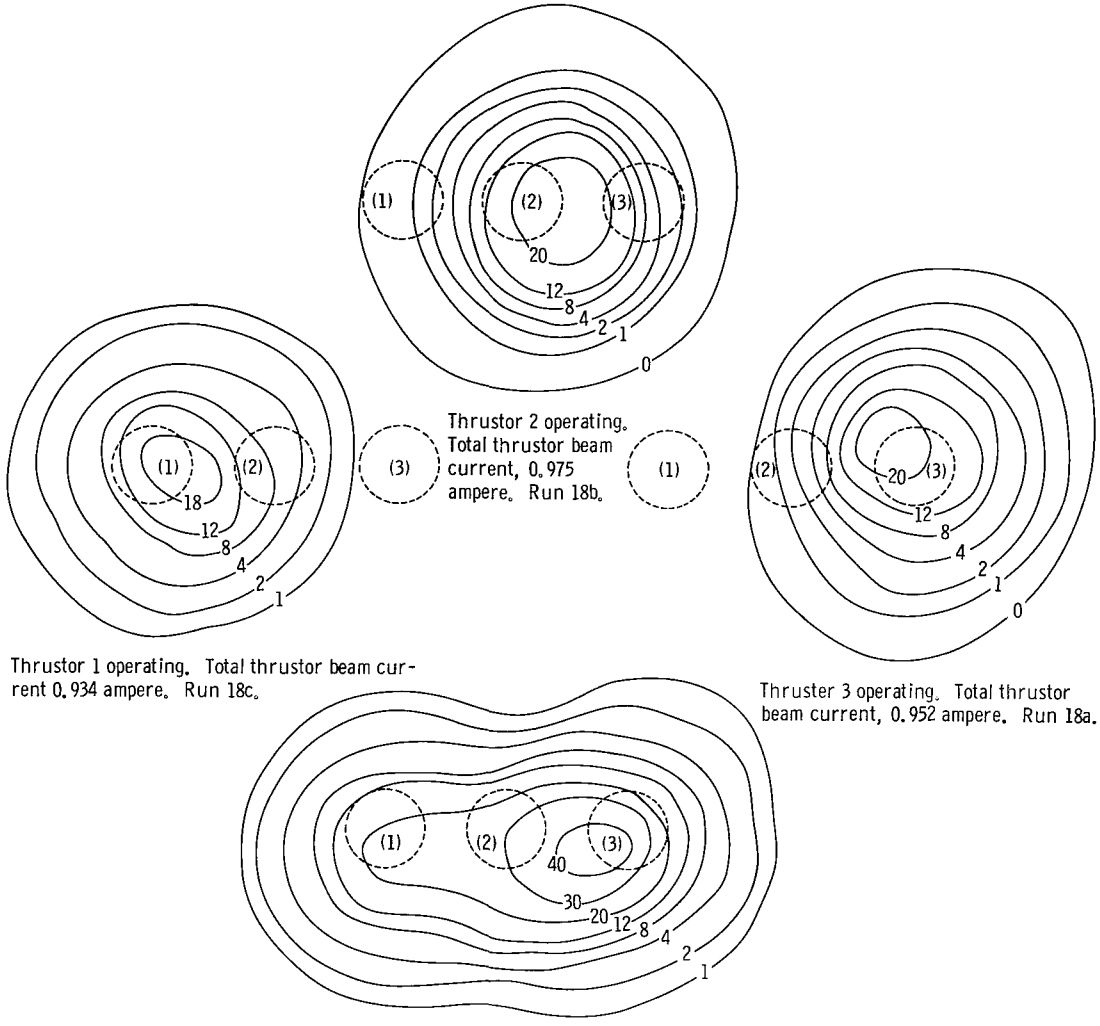

(d) Thrustors operating near 1.00 ampere beam current. Relative beam intensity numbers on contours correspond to 45 microamperes per unit.

Figure 15. - Concluded. Ion-beam contour maps for various modes of operation.

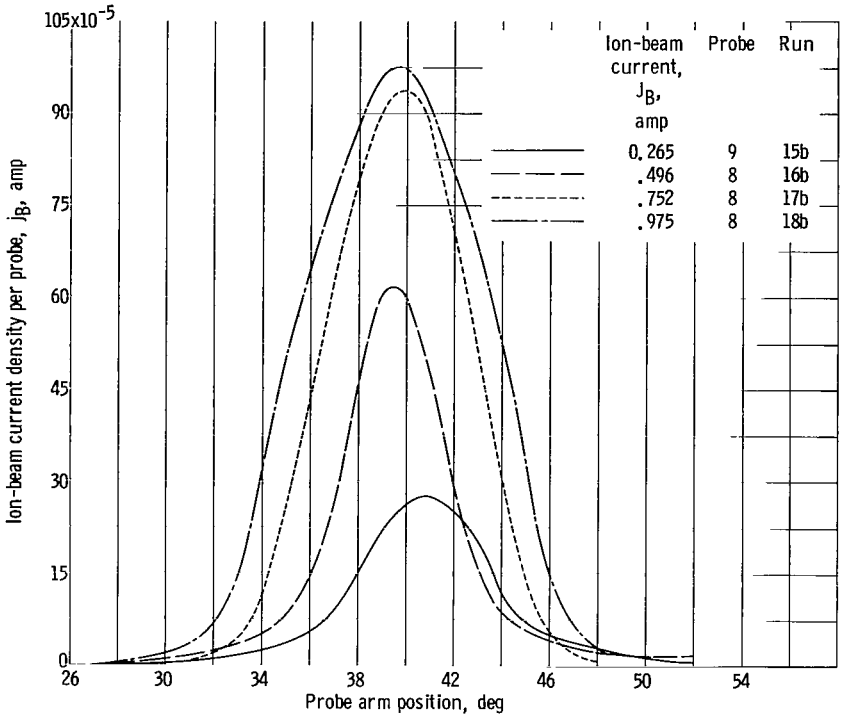

Figure 16. - Ion-beam profiles for center thrustor only.

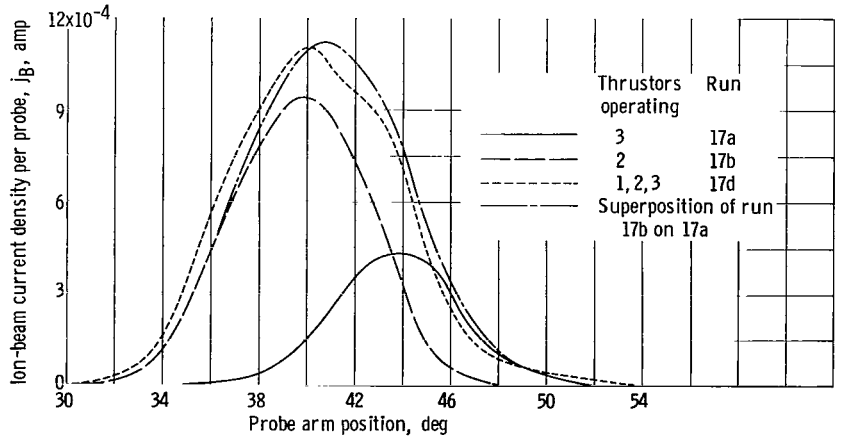

Figure 17. - Ion-beam profiles obtained from probe 8 during individual- and multiple-thrustor operation.

"The aeronautical and space activities of the United States shall be conducted so as to contribute . . . to the expansion of human knowledge of phenomena in the atmosphere and space. The Administration shall provide for the widest practicable and appropriate dissemination of information concerning its activities and the results thereof."

—NATIONAL AERONAUTICS AND SPACE ACT OF 1958

NASA SCIENTIFIC AND TECHNICAL PUBLICATIONS

TECHNICAL REPORTS: Scientific and technical information considered important, complete, and a lasting contribution to existing knowledge.

TECHNICAL NOTES: Information less broad in scope but nevertheless of importance as a contribution to existing knowledge.

TECHNICAL MEMORANDUMS: Information receiving limited distribution because of preliminary data, security classification, or other reasons.

CONTRACTOR REPORTS: Technical information generated in connection with a NASA contract or grant and released under NASA auspices.

TECHNICAL TRANSLATIONS: Information published in a foreign language considered to merit NASA distribution in English.

TECHNICAL REPRINTS: Information derived from NASA activities and initially published in the form of journal articles.

SPECIAL PUBLICATIONS: Information derived from or of value to NASA activities but not necessarily reporting the results of individual NASA-programmed scientific efforts. Publications include conference proceedings, monographs, data compilations, handbooks, sourcebooks, and special bibliographies.

Details on the availability of these publications may be obtained from:

SCIENTIFIC AND TECHNICAL INFORMATION DIVISION

NATIONAL AERONAUTICS AND SPACE ADMINISTRATION

Washington, D.C. 20546